iScience

CellPress

Article

The Transcription Factor ATF7 Controls Adipocyte Differentiation and Thermogenic Gene Programming

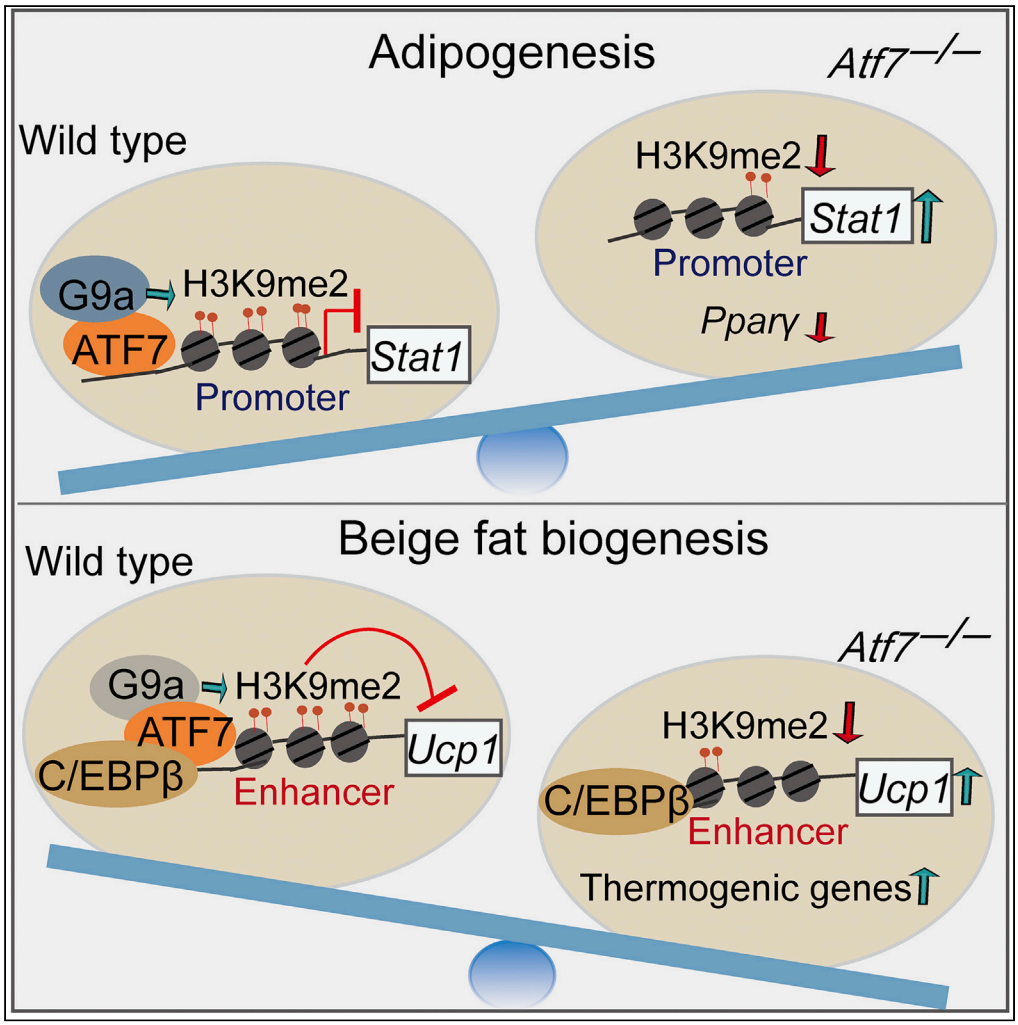

Yang Liu, Toshio Maekawa, Keisuke Yoshida, Masafumi Muratani, Bruno Chatton, Shunsuke Ishii

sishii@rtc.riken.jp

HIGHLIGHTS

ATF7 is required for adipocyte differentiation

ATF7 represses the expression of interferon-stimulated genes (ISGs) in adipocytes

Loss of ATF7 promotes the browning of inguinal white adipose tissue

ATF7 associates with C/EBPβ and G9a to silence *Ucp1* expression

DATA AND SOFTWARE AVAILABILITY

GSE122374
GSE122346

Liu et al., iScience *13*, 98–112
March 29, 2019
https://doi.org/10.1016/j.isci.2019.02.013

iScience

CellPress

Article

The Transcription Factor ATF7 Controls Adipocyte Differentiation and Thermogenic Gene Programming

Yang Liu,[1] Toshio Maekawa,[1] Keisuke Yoshida,[1] Masafumi Muratani,[3] Bruno Chatton,[4] and Shunsuke Ishii[1,2,5,*]

SUMMARY

Adipocytes function as major players in the regulation of metabolic homeostasis, and factors contributing to adipocyte differentiation and function are promising targets for combatting obesity and associated metabolic disorders. Activating transcription factor 7 (ATF7), a stress-responsive chromatin regulator, is involved in energy metabolism, but the underlying mechanisms remain unknown. Herein, we showed that ATF7 is required for adipocyte differentiation and interacts with histone dimethyltransferase G9a in adipocytes to repress the expression of interferon-stimulated genes, which in turn suppress adipogenesis. Ablation of ATF7 promotes beige fat biogenesis in inguinal white adipose tissue. ATF7 binds to transcriptional regulatory regions of the gene encoding uncoupling protein 1, silencing it by controlling histone H3K9 dimethylation. Our findings demonstrate that ATF7 is a multifunctional adipocyte protein involved in the epigenetic control of development and function in adipose tissues.

INTRODUCTION

Obesity is a major contributor to numerous metabolic diseases including type 2 diabetes, hypertension, and atherosclerosis. Adipose tissue plays an essential role in regulating the whole-body energy balance. White adipose tissue (WAT) stores excess energy as lipids, whereas brown adipose tissue (BAT) expends energy as heat. The thermogenic properties of BAT are dependent on high oxidative capacity and mitochondrial density and high levels of uncoupling protein 1 (UCP1). Classical brown adipocytes are mainly located around interscapular BAT, whereas beige adipocytes, inducible brown-fat-like cells, sporadically reside in subcutaneous WAT depots (Bartelt and Heeren, 2014). The emergence of beige adipocytes in WAT is induced by environmental stimuli, including cold exposure, exercise, long-term peroxisome proliferator-activated receptor γ (PPARγ) activation, and β-adrenergic receptor stimulation (Harms and Seale, 2013). The browning of WAT can prevent diet-induced obesity and improve metabolism (Kajimura and Saito, 2014). Notably, recent studies also suggest that these beige adipocytes can significantly contribute to the energy balance in humans (Sidossis and Kajimura, 2015).

Obesity-associated macrophage infiltration in adipose tissues is coupled with the recruitment of proinflammatory M1 macrophages, leading to increased expression of proinflammatory cytokines such as interleukin-6 (IL-6) and tumor necrosis factor alpha (TNF-α) (McLaughlin et al., 2017). These proinflammatory cytokines induce an inflammatory phenotype in adipocytes and prevent adipogenesis of 3T3-L1 cells (Gustafson and Smith, 2006). Elevated circulating lipopolysaccharide (LPS) levels in obesity also trigger inflammation in macrophages and preadipocytes of adipose tissues, and LPS treatment inhibits differentiation of adipocyte precursors *in vitro* (Zhao and Chen, 2015). In addition to LPS, interferon-α (IFN-α), a key stimulator of the innate immune response, inhibits adipogenesis of 3T3-L1 cells (Lee et al., 2016). Thus, accumulating evidence indicates that activation of innate immune responses negatively regulates adipocyte differentiation. However, the molecular players that repress innate immune responses in adipocytes remain elusive.

Activating transcription factor 7 (ATF7) belongs to the vertebrate ATF2 subfamily of transcription factors, which has three members: ATF2 (originally named CRE-BP1) (Maekawa et al., 1989; Hai et al., 1989), CRE-BPa (Nomura et al., 1993), and ATF7 (originally named ATFa) (Gaire et al., 1990). ATF2 proteins reportedly contribute to the regulation of adipocyte differentiation and function. *Atf2*$^{+/-}$*Cre-bpa*$^{+/-}$ double-heterozygous mice exhibit reduced WAT mass, and bone morphogenetic protein 2 can induce the p38-dependent phosphorylation of ATF2, which binds to the promoter region of *Pparγ2* to stimulate adipocyte

[1]RIKEN Cluster for Pioneering Research, Tsukuba, Ibaraki 305-0074, Japan

[2]Graduate School of Comprehensive Human Sciences, University of Tsukuba, Tsukuba, Ibaraki 305-8577, Japan

[3]Department of Genome Biology, Faculty of Medicine, University of Tsukuba, Tsukuba, Ibaraki 305-8575, Japan

[4]Université de Strasbourg, UMR7242 Biotechnologie et Signalisation Cellulaire, Ecole Supérieure de Biotechnologie de Strasbourg, BP10413 Illkirch, France

[5]Lead Contact

*Correspondence: sishii@rtc.riken.jp

https://doi.org/10.1016/j.isci.2019.02.013

differentiation (Maekawa et al., 2010a). The p38-dependent activation of ATF2 is also required for the induction of thermogenic genes, including *Ucp1* (Cao et al., 2004), *Pgc1α* (Bordicchia et al., 2012; Yao et al., 2017), and *Zfp516* (Dempersmier et al., 2015), in BAT in response to various stimuli. Although ATF7 shares a relatively high amino acid sequence identity with ATF2, it represses rather than activating, gene expression in the absence of stress (Seong et al., 2012). ATF7 recruits histone methyltransferases to silence the transcription of target genes. Histone H3K9 trimethyltransferase ESET/SETDB1 is recruited by ATF7 to promote the formation of heterochromatin-like structure on the regulatory region of the *Htr5b* gene, which encodes serotonin receptor 5b, in the dorsal raphe nuclei of the brain (Maekawa et al., 2010b). Social isolation stress induces the phosphorylation of ATF7 via p38 and leads to the release of ATF7 and ESET/SETDB1 from target genes, resulting in transcriptional activation. ATF7 represses a group of innate immunity-related genes in macrophages by associating with H3K9 dimethyltransferase G9a. Pathogen-infection-induced phosphorylation of ATF7 stimulates the release of ATF7-G9a from target genes, accompanied by a decrease in repressive histone H3K9me2 levels, leading to elevated gene expression (Yoshida et al., 2015). In mouse embryonic fibroblast cells, ATF7 regulates H3K9me3 levels on pericentromeric heterochromatin and telomeres by interacting with Suv39h1 (Maekawa et al., 2018).

Our previous study found that deletion of *Atf7* reduced adipose tissue mass and increased energy expenditure in mice fed a high-fat diet (Liu et al., 2016), implying that ATF7 may participate in the regulation of energy balance. In the present work, we have more precisely analyzed the role of ATF7 in adipocyte differentiation and showed that ATF7 facilitates adipogenesis by repressing innate immune responses, whereas it suppresses beige adipocyte biogenesis via dimethylation of H3K9 on thermogenic gene enhancers. Thus ATF7 has a dual role for the regulation of white adipocyte differentiation and beige fat biogenesis in inguinal white adipose tissue (iWAT).

RESULTS

ATF7 Deficiency Impairs Adipocyte Differentiation

Atf7-deficient (*Atf7*$^{-/-}$) mice exhibited reduced adipose tissue mass, suggesting that ATF7 may contribute to adipocyte differentiation (Liu et al., 2016). To investigate the function of ATF7 in the regulation of adipocytes, we examined whether ATF7 was expressed in fat tissues. ATF7 was detected in BAT, iWAT, and epididymal WAT (Figure 1A). The stroma-vascular fraction (SVF) of adipose tissues provides a rich reservoir of adipocyte precursors. We measured the expression levels of *Atf7*, *Wnt10b*, and *Prdm16* genes in isolated mature adipocytes and the SVF from BAT and iWAT. *Wnt10b* expression decreases during adipocyte differentiation (Cawthorn et al., 2012), and *Prdm16* is mainly expressed in mature adipocytes (Seale et al., 2007). In line with previous reports, we also observed that *Wnt10b* was mainly expressed in the SVF, whereas *Prdm16* exhibited higher expression levels in adipocytes than in the SVF (Figures S1A and S1B). However, there was no difference in *Atf7* gene expression in adipocytes from BAT and iWAT. ATF7 was also expressed at comparable levels in the SVF and mature adipocytes (Figure 1B). To explore the expression of *Atf7* during adipocyte differentiation, we used inguinal primary preadipocytes and measured gene expression by quantitative PCR (qPCR). The results indicated that *Atf7* expression was reduced by 40% (day 2) after cells were cultured in induction medium, and expression then increased to day 0 levels, whereas expression of the adipogenesis marker *Fabp4* gradually increased during adipocyte differentiation (Figure 1C).

To determine the function of ATF7 in adipocyte differentiation, we used primary inguinal preadipocytes isolated from wild-type (WT) and *Atf7*$^{-/-}$ mice to examine whether loss of ATF7 affects adipogenesis. ATF7 ablation reduced the number of oil red O-stained mature adipocytes (Figure 1D), and the expression level of adipogenic markers *Pparγ*, *C/ebpα*, and *Fabp4* (Figures 1E and 1G). By contrast, *C/ebpβ* expression levels were not affected by ATF7 deficiency (Figure 1E). When cells were induced to undergo adipocyte differentiation in the presence of the PPARγ agonist rosiglitazone (Rosi), which promotes adipogenesis and activates brown-selective genes (Schoonjans et al., 1996), *Atf7* expression exhibited similar changes to those observed in the absence of Rosi, indicating that this agent did not affect *Atf7* expression (Figures S2A and S2B). Notably, the presence of Rosi rescued ATF7-deficiency-induced impairment of adipogenesis. Oil red O staining revealed no difference in lipid accumulation between WT and *Atf7*$^{-/-}$ cells cultured with Rosi (Figure 1F). Rosi dramatically up-regulated *Fabp4* expression in both WT and ATF7 knockout (KO) cells, and importantly, *Fabp4* expression in ATF7 KO cells was comparable to that in WT cells in the presence of Rosi (Figure 1G). Compared with WT cells, the common adipogenic markers *Pparγ*, *C/ebpα*, and *C/ebpβ* also exhibited similar expression levels in *Atf7*$^{-/-}$ cells when treated with Rosi

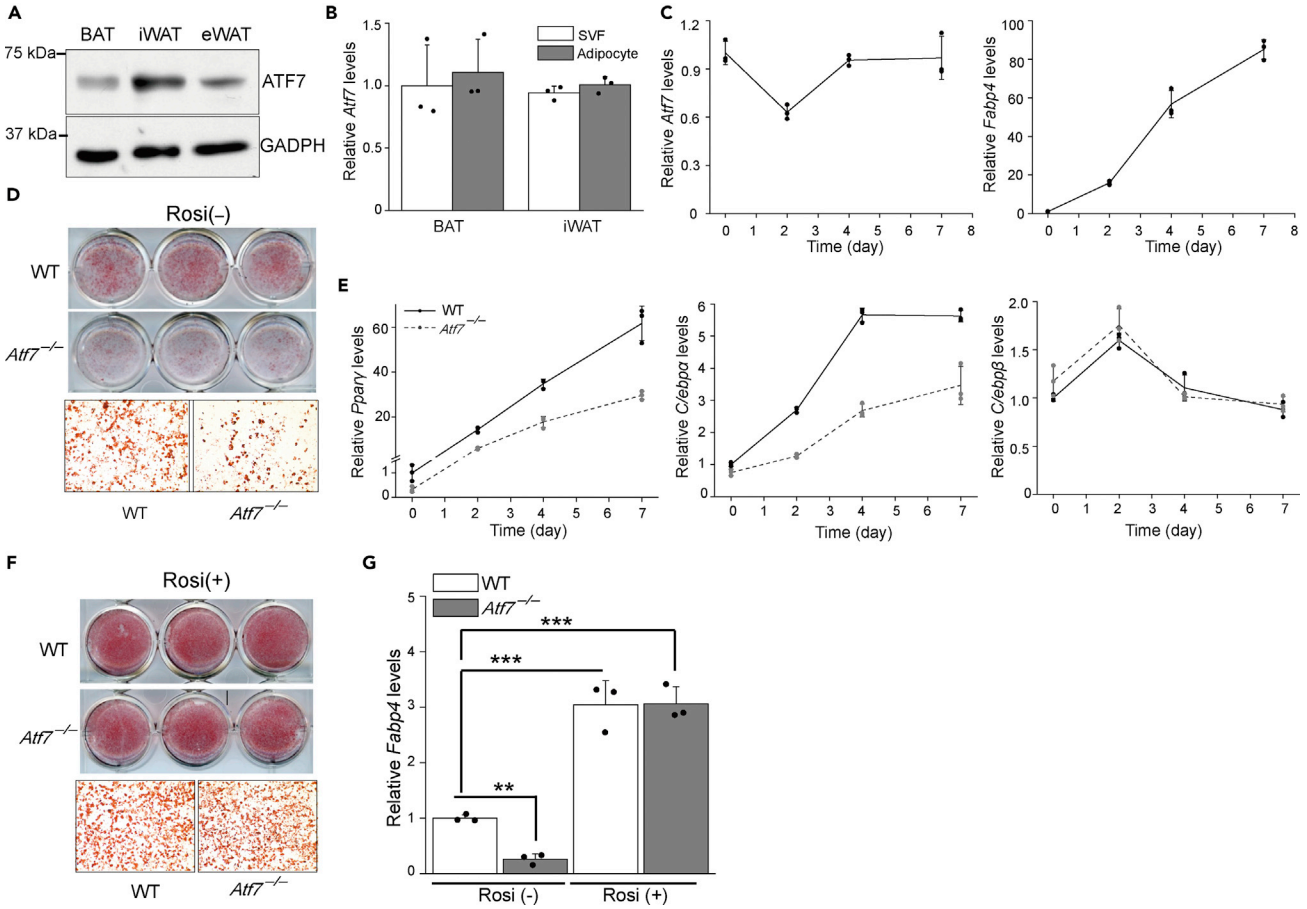

Figure 1. Loss of ATF7 Impairs Adipogenesis

(A) ATF7 protein expression levels in BAT, iWAT, and epididymal WAT measured by immunoblotting.

(B) *Atf7* mRNA expression levels in mature adipocytes and stromal vascular cells isolated from BAT and iWAT (n = 3, three biological replicates). Data are presented as mean ± SD. Statistical analysis was performed using two-tailed unpaired Student's t tests.

(C) *Atf7* (left) and *Fabp4* (right) gene expression during the differentiation time course of primary iWAT preadipocytes (n = 3, three biological replicates).

(D) Oil red O staining of wild-type (WT) and *Atf7*$^{-/-}$ primary iWAT preadipocytes at 7 days after induction of differentiation in the absence of rosiglitazone (Rosi).

(E) Expression of the common adipogenic genes *Pparγ*, *C/ebpα*, and *C/ebpβ*, detected by real-time PCR during the differentiation time course of WT and *Atf7*$^{-/-}$ primary iWAT preadipocytes (n = 3, three biological replicates).

(F) Oil red O staining of WT and *Atf7*$^{-/-}$ primary iWAT preadipocytes at 7 days after induction of differentiation in the presence of Rosi.

(G) *Fabp4* gene expression levels in differentiated WT and *Atf7*$^{-/-}$ primary iWAT preadipocytes in the presence or absence of Rosi.

Data are presented as means ± SD. Statistical analysis was performed using two-way ANOVA followed by Holm-Sidak multiple comparison tests. *$p < 0.05$, **$p < 0.01$, ***$p < 0.001$ versus WT (without Rosi treatment). See also Figures S1 and S2.

(Figure S2C). These findings indicate that ATF7 negatively regulates adipogenesis, directly or indirectly, by repressing *Pparγ* expression.

ATF7 Represses Innate Immune-Related Genes in Adipocytes

To investigate the mechanism by which ATF7 suppresses adipogenesis, we performed RNA sequencing (RNA-seq) on adipocytes (D7) derived from inguinal preadipocytes in the presence and absence of Rosi. In the absence of Rosi, 673 genes were up-regulated and 237 genes were down-regulated by the loss of ATF7, and Gene Ontology analysis revealed that up-regulated genes were related to immune responses (Figure 2A). The most enriched pathways associated with these up-regulated genes included innate immune responses, defense responses to viruses, and cellular responses to IFN-β, whereas the down-regulated genes were mainly related to lipid metabolism and storage (Figure S3A). We also identified 200 genes that were up-regulated and 174 genes that were down-regulated in *Atf7*$^{-/-}$ cells compared with WT cells in

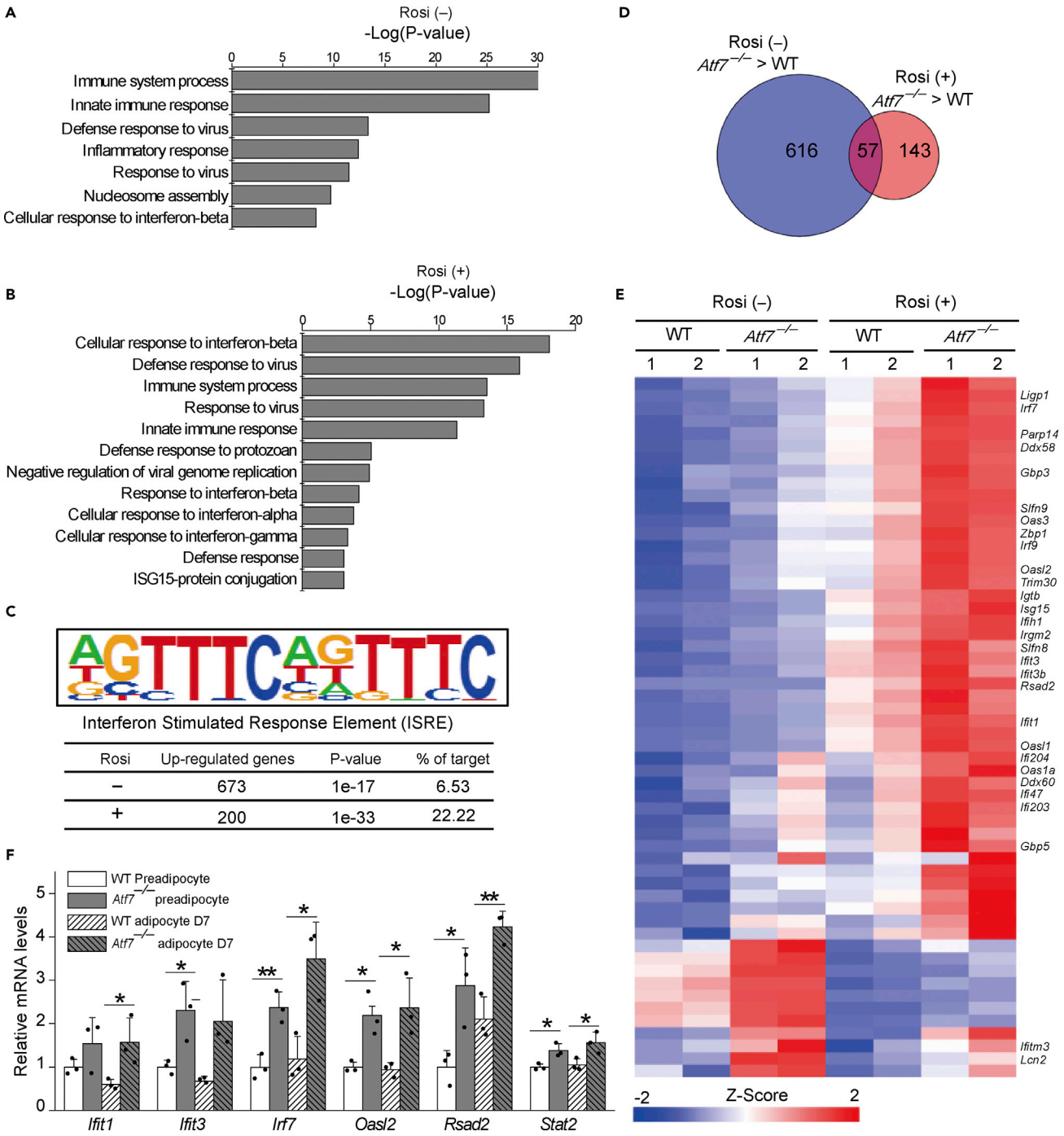

Figure 2. ATF7 Represses Innate Immune Gene Expression in Adipocytes

(A and B) Gene Ontology (GO) pathways (Biological Process category) enriched in up-regulated genes in differentiated *Atf7*$^{-/-}$ primary iWAT preadipocytes compared with WT controls in the absence (A) or presence (B) of rosiglitazone (Rosi).

(C) The interferon-stimulated response element (ISRE)-binding motif is the most enriched DNA motif within the promoters of up-regulated genes induced by loss of ATF7 in differentiated adipocytes.

(D) Venn diagram showing the number of overlapping up-regulated genes in *Atf7*$^{-/-}$ cells in the presence and absence of Rosi.

(E) Heatmap depicting the expression levels of overlapping up-regulated genes in WT and *Atf7*$^{-/-}$ cells (n = 2, two biological replicates).

(F) Gene expression levels of IFN-stimulated genes (ISGs) in WT and *Atf7*$^{-/-}$ primary preadipocytes and differentiated adipocytes at day 7 (D7, n = 3, three biological replicates).

Data are presented as means ± SD. Statistical analysis was performed using two-tailed unpaired Student's t tests. *p < 0.05, **p < 0.01. See also Figures S3–S5.

the presence of Rosi, and down-regulated genes were related to positive regulation of angiogenesis, negative regulation of insulin secretion, and cellular response to IL-1 and TNF-α (Figure S3B). Interestingly, pathway analysis for up-regulated genes gave similar results to those obtained from adipocytes cultured without Rosi (Figure 2B). These up-regulated genes were also mainly associated with immune response pathways, implying that ATF7 may inhibit immune-related gene expression in adipocytes.

To clarify the factors potentially modulating these up-regulated genes in *Atf7*$^{-/-}$ adipocytes, we performed motif analysis of promoter regions and found that interferon-stimulated response element (ISRE) was the most enriched motif in genes up-regulated in *Atf7*$^{-/-}$ cells in both the presence and absence of Rosi. Without Rosi, 6.53% of the 673 gene promotors contain an ISRE, and in the presence of Rosi, this ratio increases to 22.22% (Figure 2C). Furthermore, 57 genes overlap between the two up-regulated gene sets, including many interferon-stimulated genes (ISGs) such as *Irf7*, *Ifit1*, *Ifit3*, *Rsad2*, and *Oasl2* (Figures 2D and 2E). In accordance with the RNA-seq data, the results of qPCR demonstrated that ISGs were more highly expressed in *Atf7*$^{-/-}$ adipocytes (D7), and they were also increased in *Atf7*$^{-/-}$ preadipocytes compared with WT controls (Figure 2F). To further validate the role of ATF7 in the regulation of ISG expression, we overexpressed ATF7 in the C3H10T1/2 murine mesenchymal stem cell line (Figure S4A). Expression of ISGs was stimulated by treatment with LPS (0.5 μg/mL) for 12 h. However, overexpression of ATF7 significantly repressed ISG expression in the absence and presence of LPS (Figure S4B). Taken together, these results suggest that ATF7 suppresses the induction of ISGs, and loss of ATF7 stimulates ISG expression during adipocyte differentiation.

In contrast to *in vitro* data, the results of qPCR and immunofluorescence staining demonstrated that loss of ATF7 did not affect the inflammation level of iWAT (Figures S5A and S5B). Interestingly, we found that loss of ATF7 led to a dramatic reduction in the *Retn* gene expression in adipocytes (Figure S5C). This finding was consistent with the lower circulating resistin observed in the *Atf7*$^{-/-}$ mice (Liu et al., 2016). Given the pro-inflammatory properties of resistin in adipose tissue (Qatanani et al., 2009), the reduction of resistin may counter the adipose tissue inflammation induced by the activation of innate immune response in *Atf7*$^{-/-}$ adipocytes. These results suggest that ISGs are up-regulated in *Atf7*$^{-/-}$ adipocytes, but it does not cause the inflammation at the tissue level because of negative feedback regulation by resistin.

Activation of ISGs Impairs Adipogenesis

To examine the effect of the induction of ISGs on adipogenesis, we treated preadipocytes with LPS (0.5 μg/mL) for 24 h and found that LPS treatment dramatically stimulated the expression of ISGs (Figure S6A). By contrast, *Pparγ* expression levels in LPS-treated cells were reduced by approximately half compared with those in phosphate-buffered saline (PBS)-treated control cells (Figure S6B), implying that LPS treatment may impair adipogenesis by repressing *Pparγ* expression. A previous study demonstrated that LPS treatment for 24 h before the induction of adipocyte differentiation results in the profound impairment of adipogenesis (Zhao and Chen, 2015). In line with these previous observations, we also found that adipocyte differentiation was severely blunted by LPS exposure for 24 h before addition of induction medium. In the absence of Rosi, LPS treatment led to decreased lipid accumulation and lower expression levels of adipogenic markers (Figures S6C and S6D). Interestingly, the presence of Rosi during differentiation clearly rescued the impairment of adipogenesis induced by LPS treatment. The results of oil red O staining demonstrated that Rosi mitigates the effect of LPS treatment on lipid accumulation (Figure S6C). Moreover, there was no difference in expression levels of Pparγ between LPS- and PBS-treated cells in the presence of Rosi, although *Fabp4* and *C/ebpα* expression remained slightly reduced following LPS treatment (Figure S6D).

IFN-α can stimulate the expression of ISGs and inhibit adipogenesis in 3T3-L1 cells (Lee et al., 2016). However, the inhibitory effect of IFN-α on adipogenesis in brown adipocyte precursors was not observed (Kissig et al., 2017). To examine the effect of IFN-α on adipogenesis in iWAT preadipocytes, we measured the expression of ISGs in preadipocytes following exposure to IFN-α (500 U/mL) for 24 h and found that expression levels of ISGs *Stat1* and *Stat2* were significantly elevated by IFN-α (Figure 3A). By contrast, *Pparγ* expression levels in IFN-α-treated cells were reduced by 80% compared with those in control cells (Figure 3B). Exposure to IFN-α during adipocyte differentiation severely inhibited lipid accumulation and expression of adipogenic markers (Figure 3C and 3D). Taken together, these results indicate that induction of ISGs by LPS and IFN-α is accompanied by a reduction in *Pparγ* expression, leading to inhibition of adipogenesis.

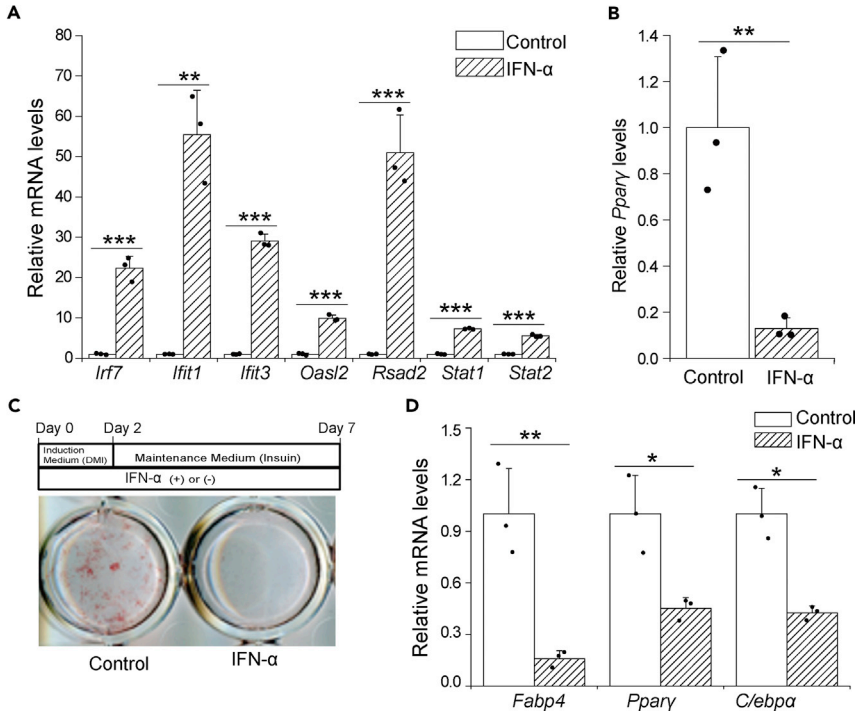

Figure 3. IFN-α Inhibits Adipocyte Differentiation of Primary iWAT Preadipocytes

(A) Induction of ISG expression in preadipocytes by IFN-α treatment (n = 3, three biological replicates).

(B) Relative mRNA levels are reduced by IFN-α treatment in preadipocytes (n = 3, three biological replicates).

(C) Oil red O staining of differentiated preadipocytes in the presence or absence of IFN-α.

(D) Expression levels of adipogenic genes *Fabp4*, *Pparγ*, and *C/ebpα* in differentiated pre-adipocytes with or without IFN-α treatment (n = 3, three biological replicates).

Data are presented as means ± SD. Statistical analysis was performed using two-tailed unpaired Student's t tests. *p < 0.05, **p < 0.01, ***p < 0.001. See also Figures S6.

ATF7 Recruits G9a to Repress *Stat1* Expression in Preadipocytes

Given that ATF7 associates with histone dimethyltransferase G9a to suppress the expression of innate immune-related genes in macrophages (Yoshida et al., 2015), we speculated that inhibition of ISG expression in adipocytes by ATF7 may occur in the same manner. To test this hypothesis, we first compared genes up-regulated by loss of ATF7 in macrophages and adipocytes. Among the top 250 genes up-regulated in *Atf7*$^{-/-}$ macrophages, 58 also exhibited higher expression levels in *Atf7*$^{-/-}$ adipocytes than in WT controls (Figure S7A). Pathway analysis of these 58 overlapping genes revealed their association with innate immune responses (Figure S7B). To examine whether ATF7 inhibits the expression of ISGs via recruitment of G9a, we performed a co-immunoprecipitation (coIP) experiment in preadipocytes using anti-ATF7 antibody. The results demonstrated that ATF7 does indeed form a complex with endogenous G9a in preadipocytes (Figure 4A).

STAT1 functions as a master regulator of the induction of ISGs by binding to ISREs. In macrophages, ATF7 directly binds the promoter region of *Stat1* to repress its expression (Yoshida et al., 2015). Thus we speculated that *Stat1* may also be a target gene of ATF7 in preadipocytes. Chromatin immunoprecipitation-qPCR results confirmed that ATF7 binds directly to the promoter of the *Stat1* gene in preadipocytes (Figure 4B). Importantly, the loss of ATF7 led to lower H3K9me2 levels at the promoter region of the *Stat1* gene, and increased expression of *Stat1* in *Atf7*$^{-/-}$ preadipocytes (Figures 4C and 4D). These findings imply that ATF7 may recruit G9a to the promoter region of *Stat1* and repress its expression through dimethylation of H3K9 in preadipocytes. Elevated STAT1 induced by loss of ATF7 in turn stimulates the expression of ISGs and inhibits adipogenesis.

Loss of ATF7 Promotes the Thermogenic Programming and Browning of iWAT

The PPARγ agonist Rosi induces thermogenic gene programming of beige and brown adipocytes (Ohno et al., 2012). RNA-seq data showed that the majority of BAT-selective genes, including *Ucp1*, *Cidea*, *Pparα*,

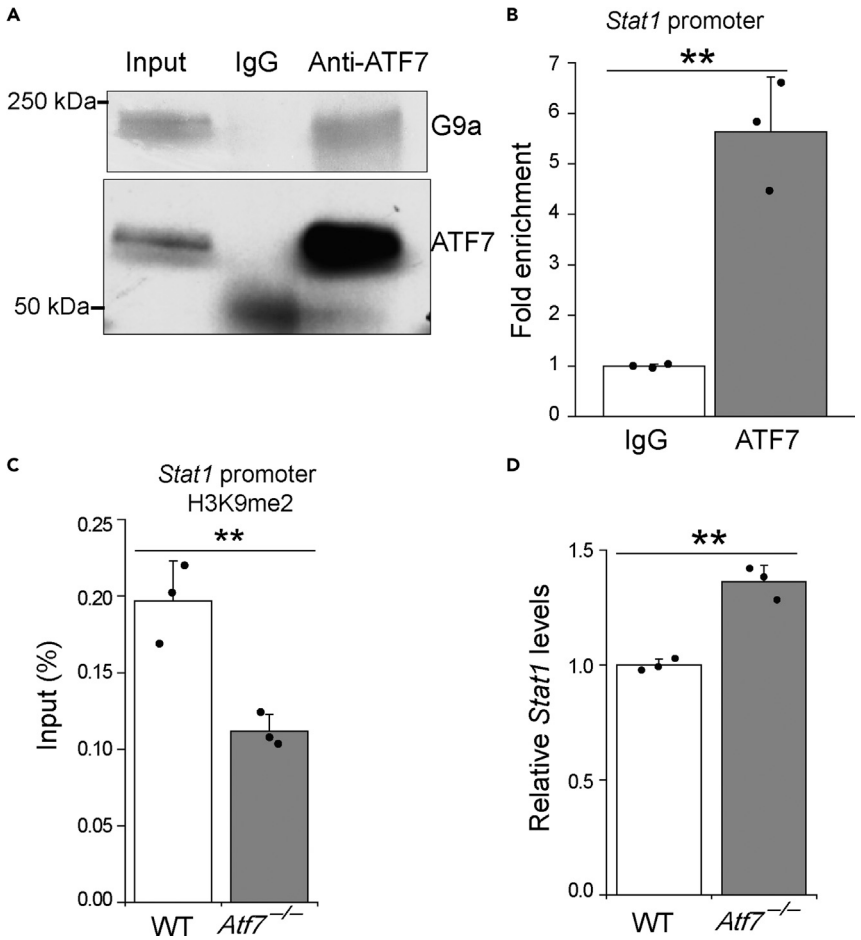

Figure 4. ATF7 Recruits G9a to Repress Stat1 Expression in Preadipocytes

(A) Cell extracts of preadipocytes were immunoprecipitated with antibody (2F10)-recognizing ATF7 and immunoblotted with antibody against G9a.

(B) Chromatin immunoprecipitation-qPCR analysis showing the binding of ATF7 to the *Stat1* gene promoter (n = 3, three biological replicates).

(C) H3K9me2 enrichment on the *Stat1* promoter in WT and *Atf7*$^{-/-}$ preadipocytes (n = 3, three biological replicates).

(D) Relative *Stat1* mRNA levels in WT and *Atf7*$^{-/-}$ preadipocytes (n = 3, three biological replicates).

Data are presented as means ± SD. Statistical analysis was performed using two-tailed unpaired Student's t tests. **p < 0.01. See also Figures S7.

and *Otop1*, were evidently stimulated by Rosi treatment in both WT and *Atf7*$^{-/-}$ cells (Figure 5A). Interestingly, *Ucp1* exhibited higher expression in *Atf7*$^{-/-}$ cells than in WT cells in the presence of Rosi (Figure 5B). Other thermogenic genes, such as *Cidea*, *Cox8b*, and *Pgc1α*, were also increased by the loss of ATF7, whereas *Prdm16* expression was not significantly different between WT and *Atf7*$^{-/-}$ cells (Figure 5C). The acute stimulation of thermogenic genes in response to the activation of β-adrenergic receptors is one of the main functional characteristics of beige/brown adipocytes. To examine whether ATF7 is essential for this, differentiated WT and *Atf7*$^{-/-}$ cells were treated with isoproterenol (Iso), a synthetic pan β-adrenergic receptor agonist. *Ucp1* expression levels were significantly increased in both WT and *Atf7*$^{-/-}$ cells after Iso exposure for 4 h (Figure 5D). Of note, the increase in *Ucp1* expression stimulated by Iso was comparable in WT and *Atf7*$^{-/-}$ cells (~4-fold), implying that ATF7 may be dispensable for activation of beige cells via β-adrenergic receptors. These findings indicate that loss of ATF7 promotes thermogenic programming in a cell-autonomous manner.

To determine whether ATF7 contributes to thermogenic programming of beige or brown adipocyte *in vivo*, we examined UCP1 protein levels in BAT and iWAT in WT and *Atf7*$^{-/-}$ mice. We found that loss of ATF7 did

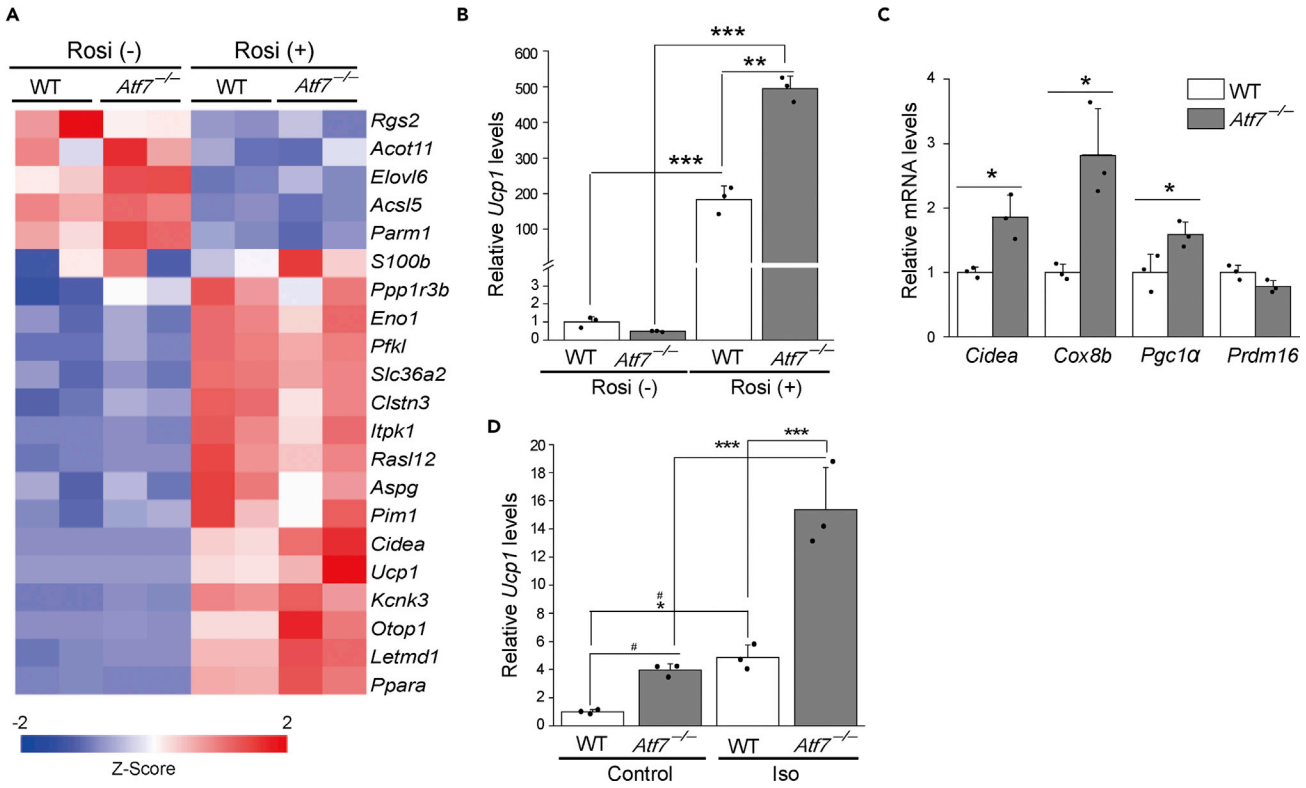

Figure 5. Loss of ATF7 Promotes Thermogenic Gene Programming

(A) Heatmap showing the expression levels of BAT-selective genes in WT and *Atf7*$^{-/-}$ cells in the presence or absence of rosiglitazone (Rosi; n = 2, two biological replicates).

(B) *Ucp1* gene expression levels in WT and *Atf7*$^{-/-}$ differentiated primary iWAT preadipocytes in the presence or absence of Rosi (n = 3, three biological replicates). Data are presented as means ± SD. Statistical analysis was performed using two-way ANOVA followed by Holm-Sidak multiple comparison tests. **p < 0.01, ***p < 0.001.

(C) Thermogenic gene expression levels in differentiated WT and *Atf7*$^{-/-}$ primary iWAT preadipocytes treated with Rosi (n = 3, three biological replicates). Data are presented as means ± SD. Statistical analysis was performed using two-tailed unpaired Student's t tests. *p < 0.05.

(D) Relative mRNA levels of *Ucp1* in differentiated WT and *Atf7*$^{-/-}$ primary iWAT preadipocytes before and after treatment with 2 μM isoproterenol (Iso) for 4 h (n = 3, three biological replicates). Data are presented as means ± SD. Statistical analysis was performed using two-way ANOVA followed by Holm-Sidak multiple comparison tests. *p < 0.05, ***p < 0.001 versus WT (no Iso treatment).

not affect UCP1 abundance in BAT, but UCP1 expression was increased in iWAT in *Atf7*$^{-/-}$ mice compared with WT controls (Figure 6A). To assess the morphology of adipocytes in iWAT, we performed hematoxylin and eosin staining of iWAT sections, and more multilocular adipocytes were observed in iWAT from *Atf7*$^{-/-}$ mice than from WT controls (Figure 6B). Importantly, immunohistochemical staining showed that the number of UCP1-positive cells was markedly increased by ablation of ATF7, consistent with evaluated UCP1 protein levels in iWAT from ATF7 KO cells (Figures 6A and 6B). To explore gene expression profiles in iWAT induced by the loss of ATF7, we performed microarray analysis using RNA isolated from iWAT in *Atf7*$^{-/-}$ and WT control cells. The results revealed that 115 genes, including *Ucp1*, *Cidea*, *Pgc1α*, and *Pparα*, were up-regulated in *Atf7*$^{-/-}$ iWAT compared with control tissue (Figure 6C). Pathway analysis revealed that these genes are associated with adaptive thermogenesis and fatty acid metabolism (Figure 6D). Subsequent qPCR results further confirmed that several brown-fat-selective genes including *Ucp1*, *Cidea*, *Pparα*, and *Ntrk3*, and mitochondrial genes including *Cox7a1* and *Cox8b*, were increased in iWAT following loss of ATF7, whereas there was no change in the expression of common adipocyte genes including *C/ebpα*, *Fabp4*, and *Pparγ* (Figure 6E). However, except for *Ntrk3*, expression of brown-fat-selective genes did not differ between WT and *Atf7*$^{-/-}$ BAT. In addition, there were no changes in the expression of mitochondrial and common adipocyte genes in *Atf7*$^{-/-}$ BAT compared with WT controls (Figure S8A). In line with the results of thermogenic gene expression in BAT, there is no significant difference in the tolerance to acute cold exposure between *Atf7*$^{-/-}$ and WT littermates (Figure S8B). Taken together, the *in vivo* and

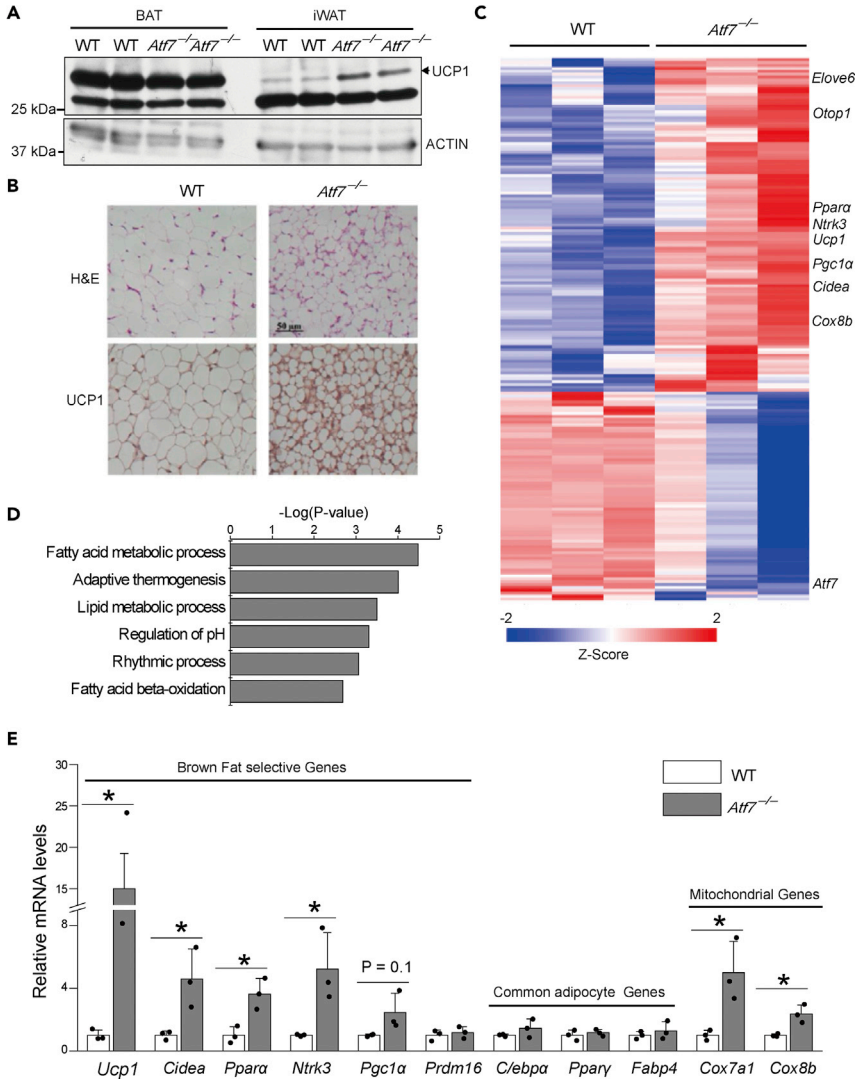

Figure 6. ATF7 Ablation Promotes Browning of iWAT

(A) Relative UCP1 protein levels in BAT and iWAT of WT and *Atf7*$^{-/-}$ littermates (n = 2, two biological replicates).

(B) Hematoxylin and eosin staining (upper) and UCP1 immunohistochemical analysis (lower) of iWAT from WT and *Atf7*$^{-/-}$ littermates.

(C) Heatmap depicting expression levels of differentially expressed genes induced by loss of ATF7 in WT and *Atf7*$^{-/-}$ littermates (n = 3, three biological replicates).

(D) Pathway analysis for up-regulated genes in *Atf7*$^{-/-}$ iWAT.

(E) Expression of brown-fat-selective genes, common adipocyte genes, and mitochondrial genes in iWAT from WT and *Atf7*$^{-/-}$ littermates (n = 3, three biological replicates).

Data are presented as means ± SD. Statistical analysis was performed using two-tailed unpaired Student's t tests. *p < 0.05. See also Figures S8.

in vitro results suggest that ATF7 contributes to the regulation of beige adipocyte biogenesis by suppressing thermogenic gene programming.

Overexpression of ATF7 Inhibits Thermogenic Gene Programming

To further explore the molecular mechanism of ATF7 functions in beige cell biogenesis, we used C3H10T1/2 multipotent mesenchymal cells, which have the capacity to undergo brown or beige adipogenic differentiation when treated with an adipogenic cocktail. The results revealed no obvious change in ATF7 protein abundance during differentiation, but phosphorylation of ATF7 was induced during the later stages of

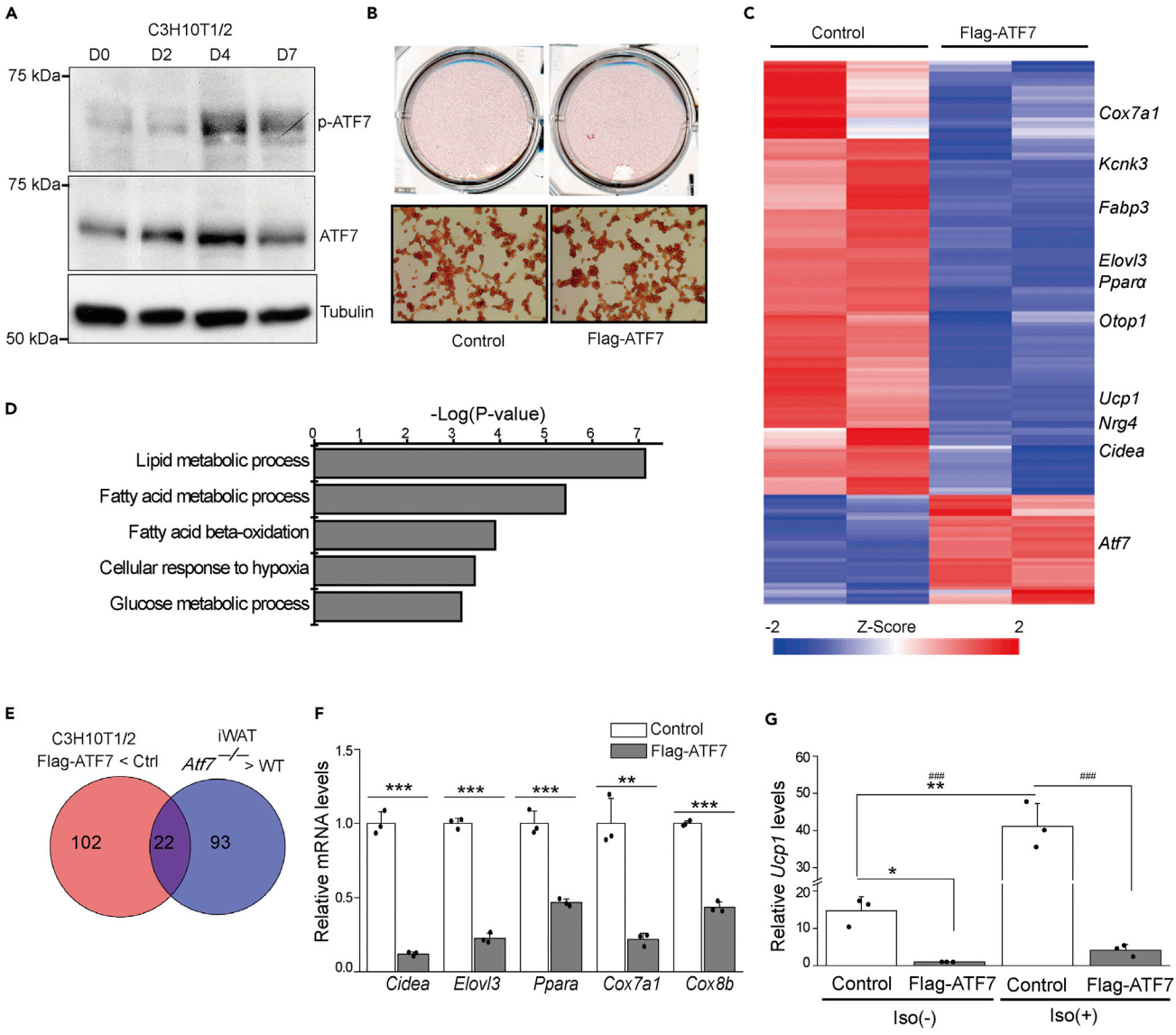

Figure 7. Overexpression of ATF7 Represses Thermogenic Gene Programming

(A) ATF7 protein and phosphorylation levels during C3H10T1/2 cell differentiation measured by immunoblotting using antibodies against ATF7 (1A7) and Phospho-ATF7 (Thr53), respectively.

(B) Oil red O staining of control and ATF7-overexpressing cells 7 days after induction of differentiation.

(C) Heatmap depicting expression levels of differentially expressed genes in ATF7-overexpressing C3H10T1/2 cells compared with control cells (n = 2, two biological replicates).

(D) Pathway analysis for down-regulated genes induced by ATF7 overexpression.

(E) Venn diagram showing the number of overlapping up-regulated genes in *Atf7*$^{-/-}$ iWAT and down-regulated genes in ATF7-overexpressing cells.

(F) Relative mRNA levels of thermogenic genes in differentiated control and ATF7-overexpressing cells (n = 3, three biological replicates). Data are presented as means ± SD. Statistical analysis was performed using two-tailed unpaired Student's t tests. **p < 0.01, ***p < 0.001.

(G) *Ucp1* gene expression levels before and after treatment with 2 μM isoproterenol (Iso) for 4 h in control and ATF7-overexpressing cells (n = 3, three biological replicates). Data are presented as means ± SD. Statistical analysis was performed using two-way ANOVA followed by Holm-Sidak multiple comparison tests. *p <0.05, **p < 0.01 versus controls (without Iso treatment), ***p < 0.001 versus controls (with Iso treatment).

differentiation (Figure 7A). To examine the role of ATF7 in differentiation, FLAG-tagged ATF7 was expressed in C3H10T1/2 cells via a lentiviral vector, and overexpression of ATF7 did not affect lipid accumulation, as shown by oil red O staining (Figure 7B). However, RNA-seq data indicated that expression of brown-fat-selective genes, including *Ucp1*, *Cidea*, *Pparα*, *Kcnk3*, and *Otop1*, was reduced following overexpression of ATF7 (Figure 7C). Notably, these down-regulated genes induced by ATF7 overexpression are

related to fatty acid and lipid metabolism (Figure 7D), similar to the pathways associated with genes up-regulated in *Atf7*$^{-/-}$ iWAT (Figure 6D). We next compared genes down-regulated by ATF7 overexpression in differentiated C3H10T1/2 cells and up-regulated by ATF7 ablation in iWAT. As shown in the Venn diagram (Figures 7E), 22 genes including *Ucp1*, *Cidea*, *Pparα*, and *Cox7a1* overlap between these two gene sets. The results of qPCR experiments further confirmed that ATF7 overexpression led to a reduction in the expression of brown-fat-selective genes *Cidea*, *Elovl3*, and *Pparα*, and mitochondrial genes *Cox7a1* and *Cox8b* (Figure 7F). Although overexpression of ATF7 strongly inhibited *Ucp1* expression, there was a 3-fold increase in *Ucp1* expression after Iso treatment in ATF7-overexpressing cells, whereas Iso stimulation led to a 3-fold increase in *Ucp1* expression in control cells (Figure 7G). These results further suggest that ATF7 does not participate in the acute activation of *Ucp1* via β-adrenergic stimulation.

ATF7 Associates with C/EBPβ and Regulates Histone Modification of *Ucp1* Enhancers

To explore the molecular mechanism underlying the repressive role of ATF7 in thermogenic gene programming, we examined whether ATF7 associates with PRDM16, which is the master regulator of the thermogenic gene programming. However, coIP experiment was performed using 293T cells, and the results indicated that ATF7 interacts with C/EBPβ, but not with PRDM16 (Figure 8A), implying that ATF7-induced suppression of thermogenic gene programming is likely not mediated by PRDM16. To further confirm whether ATF7 associated with C/EBPβ in the adipocytes, coIP experiment was performed using ATF7-overexpressing C3H10T1/2 cells after differentiation in the presence of Rosi for 4 days. We found that the interaction between ATF7 and endogenous C/EBPβ could be detected in the adipocytes (Figure 8B). Recent study demonstrated that C/EBPβ binds to the enhancer regions of thermogenic genes and controls their expression in response to IL-10 treatment (Lai et al., 2017; Rajbhandari et al., 2018). Although overexpression of ATF7 did not affect the binding of C/EBPβ to Ucp1 enhancers located 12, 5, and 2.5 kb upstream of transcription start sites, the elevated H3K9me2 levels on these regions were detected in the ATF7-overexpressing C3H10T1/2 cells after differentiation for 5 days (Figure 8C). As these enhancer regions contain the CRE (cAMP response element) sequence, we speculated that ATF7 may bind to these regions (Rajbhandari et al., 2018). The results of quantitative chromatin immunoprecipitation (qChIP) analysis confirmed that ATF7 directly binds to these enhancers in C3H10T1/2 cells after differentiation for 5 days (Figure 8D). We also investigated the effect of ATF7 deficiency on H3K9me2 levels on those enhancers, and levels on the enhancer located 5 kb upstream from the transcription start site in *Atf7*$^{-/-}$ primary iWAT preadipocytes were lower than in WT cells after differentiation in the presence of Rosi for 7 days (Figure 8E), indicating that ATF7 silences *Ucp1* gene expression by increasing H3K9me2 levels. Thus these findings demonstrate that ATF7 associates with C/EBPβ, binds enhancers of the *Ucp1* gene, and represses gene expression via H3K9me2.

DISCUSSION

In this study, we found that loss of ATF7 impairs adipogenesis and induces expression of innate immune-related genes. A previous study demonstrated that ATF7 represses innate immune gene expression in macrophages via modulation of H3K9 dimethylation levels at promoter regions (Yoshida et al., 2015). Consistent with this function in macrophages, our results demonstrated that ATF7 also functions as a repressive regulator of innate immune genes in preadipocytes. Interestingly, preadipocytes can act as macrophage-like immune cells and express the same cytokines as macrophages (Cousin et al., 1999). Under certain conditions, preadipocytes can be converted to macrophages, further implying that they may share the same regulatory mechanisms regarding regulation of innate immune responses (Charrière et al., 2003). We therefore predicted that the inhibitory function of ATF7 in innate immune-related gene expression in preadipocytes is mediated by association with G9a. In line with our hypothesis, deletion of G9a led to the activation of innate immune genes in brown preadipocytes, although G9a blocked adipogenesis by suppressing *Pparγ* expression (Wang et al., 2013).

Our results demonstrated that the promoter regions of up-regulated genes contain ISRE motifs that are recognized by STAT1. ATF7 directly binds to the promoter of *Stat1* and represses its transcription in preadipocytes via epigenetic regulation, implying that the inhibitory effect of ATF7 on innate immune gene expression is mainly mediated by STAT1. Of note, the JAK/STAT1 signaling pathway reportedly mediates the inhibitory effect of IFN-α on adipocyte differentiation (Lee et al., 2016). Moreover, *in vitro* studies suggest that STAT1 binds to the *Pparγ2* promoter in 3T3-L1 adipocytes and represses its transcription (Hogan and Stephens, 2001). Thus ATF7 may facilitate adipogenesis by indirectly regulating *Pparγ* expression via STAT1. Consistent with this possibility, we observed that the *Pparγ* agonist rosiglitazone could rescue impaired adipogenesis in ATF7-deficient primary cells. It was previously demonstrated that LPS treatment results in the defective adipogenic

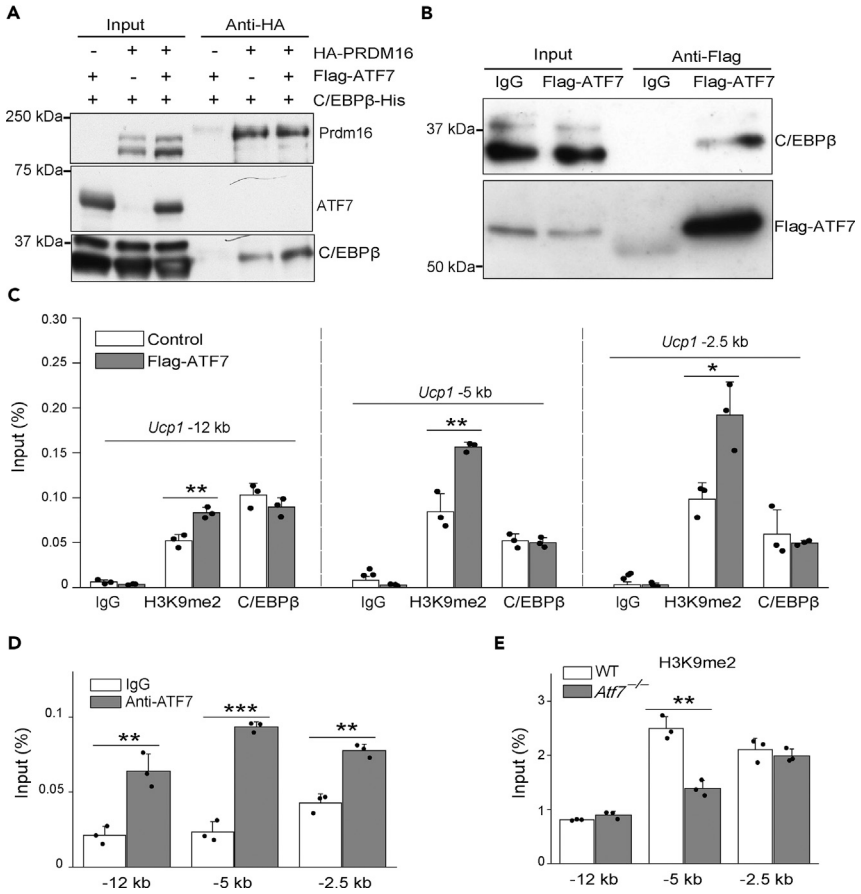

Figure 8. ATF7 Interacts with C/EBPβ and Regulates H3K9me2 Levels of *Ucp1* Enhancers

(A) 293T cells transfected with C/EBPβ-His, HA-Prdm16, and FLAG-ATF7. Lysates were immunoprecipitated with anti-hemagglutinin (HA) antibody and immunoblotted with antibodies against Prdm16, ATF7, and C/EBPβ, respectively.

(B) Co-immunoprecipitation of FLAG-ATF7 and C/EBPβ in ATF7-overexpressing C3H10T1/2 cells after differentiation in the presence of Rosi for 4 days.

(C) Chromatin immunoprecipitation (ChIP)-PCR analyses showing binding of C/EBPβ and enrichment of H3K9me2 on *Ucp1* enhancers in control and ATF7-overexpressing C3H10T1/2 cells after differentiation in the presence of Rosi for 5 days (n = 3, three biological replicates).

(D) ChIP-PCR analyses showing binding of ATF7 to *Ucp1* enhancers in differentiated C3H10T1/2 cells after differentiation in the presence of Rosi for 5 days (n = 3, three biological replicates).

(E) H3K9me2 enrichment on enhancers of *Ucp1* genes in WT and $Atf7^{-/-}$ primary iWAT preadipocytes after differentiation in the presence of Rosi for 7 days (n = 3, three biological replicates).

Data are presented as means ± SD. Statistical analysis was performed using two-tailed unpaired Student's t tests. *p < 0.05, **p < 0.01, ***p < 0.001.

potential of preadipocytes independently of nuclear factor-κB (Zhao and Chen, 2015), and phosphorylation of ATF7 in response to LPS treatment contributes to the activation of innate immune genes (Yoshida et al., 2015). Our results showed that overexpression of ATF7 blocks LPS-induced activation of innate immune genes, further suggesting that ATF7 mediates the inhibitory effect of LPS on adipogenesis.

Adipocyte differentiation and thermogenic gene programming are controlled by distinct transcriptional regulatory mechanisms, even though several common transcriptional regulators, such as TLE3 and ZFP423, are shared by these two processes. Both TLE3 and ZFP423 stimulate adipogenesis through activation of PPARγ (Villanueva et al., 2011; Gupta et al., 2010); TLE3 suppresses thermogenic gene programming by disrupting interactions between PRDM16 and PPARγ (Villanueva et al., 2013), whereas ZFP423 inhibits thermogenic gene programming by suppressing Ebf2 (Shao et al., 2016). However, ATF2 acts as a positive regulator during adipogenesis and stimulates thermogenic genes (Maekawa et al., 2010a; Cao et al., 2004).

Our results reveal that, similar to TLE3 and ZFP423, ATF7 promotes adipogenesis while inhibiting adipocyte thermogenic gene programming. Interestingly, unlike ATF2, ATF7 was found to be dispensable for acute induction of *Ucp1* by activation of β-adrenergic receptors. Although the browning of iWAT was observed in *Atf7*$^{-/-}$ mice, a difference in thermogenic gene expression in BAT was not detected. These findings suggest that ATF7 mainly contributes to the regulation of beige cell biogenesis, rather than the stimuli-induced acute enhancement of *Ucp1* expression.

Beige adipocyte biogenesis is regulated by a number of epigenetic regulators (Inagaki et al., 2016), and accumulating evidence suggests that the dynamic enhancer epigenome is tightly correlated with thermogenic gene programming in adipocytes (Roh et al., 2018; Lee et al., 2017). Notably, the amount of the repressive chromatin marker H3K9me2 on enhancers of thermogenic genes, including *Ucp1* and *Cidea*, is reduced, whereas levels of the active histone marker H3K27ac are increased during brown or beige cell biogenesis (Lai et al., 2017; Brunmeir et al., 2016). Deletion of HDAC3 in adipose tissue leads to increased H3K27 acetylation of *Ucp1* and *Pparα* enhancers, resulting in the browning of WAT (Ferrari et al., 2017). Our results showed that ATF7 associates with C/EBPβ and represses thermogenic gene programming via H3K9 dimethylation on enhancers of *Ucp1*. A recent study demonstrated that the recruitment of C/EBPβ and ATF2 is accompanied by altered histone modification on enhancer regions, which mediates the inhibitory effect of IL-10 signaling on thermogenic gene programming (Rajbhandari et al., 2018). C/EBPβ is essential for brown and beige adipocyte development through formation of a transcriptional complex with PRDM16 (Kajimura et al., 2009).

We identified that ATF7 as the transcriptional repressor of IFN signaling in adipocytes. Recent study shows that the activation of ISGs induced by IFN-α impairs the thermogenic gene programming and disrupts the mitochondrial structure in the brown adipocytes (Kissig et al., 2017). Importantly, repression of the IFN signaling by blocking of JAK-STAT pathway promotes the browning of human adipocytes (Moisan et al., 2015), highlighting the repressive role of IFN-JAK-STAT signaling in thermogenic gene expression. However, we found that loss of ATF7 promotes thermogenic gene programming, although ISGs exhibited higher level in *Atf7*$^{-/-}$ adipocytes, suggesting that ATF7 controls the expression of thermogenic genes mainly through repressive epigenetic modification on the enhancers rather than the repression of JAK-STAT pathway in adipocytes. Enhancement of beige adipocyte biogenesis by a loss of ATF7 by regulating the dimethylation of H3K9 on thermogenic gene enhancers might be more dominant compared with suppression of the same by the JAK-STAT pathway.

Expression of thermogenic genes is closely linked to environmental factors such as low temperature. Repeated cold exposure leads to increased activity in brown and beige cells, which confers beneficial effects to metabolic homeostasis (Bartelt and Heeren, 2014). A recent study indicates that paternal cold exposure before conception can enhance thermogenic gene expression in offspring by reprogramming the sperm epigenome (Sun et al., 2018). Notably, dATF2, the homolog of mammalian ATF7 in *Drosophila*, acts as a transcriptional repressor and mediates stress-induced epigenetic inheritance (Seong et al., 2011). Combined with our current results, these findings suggest that ATF7 may mediate epigenetic changes in sperm induced by cold exposure and contribute to enhanced brown or beige cell activity in the offspring of a father that experienced cold before conception.

Limitations of Study

Our results demonstrate that ATF7 can associate with C/EBPβ in adipocytes, although ATF7 may not disrupt the interaction between Prdm16 and C/EBPβ. However, at present, we cannot rule out the possibility that ATF7 blocks the association of C/EBPβ with other partners, such as the SWI/SNF complex (Kowenz-Leutz and Leutz, 1999), resulting in a reduction in C/EBPβ transcriptional activity. Furthermore, whether binding of ATF7 to enhancers of Ucp1 is dependent on C/EBPβ also needs further investigation.

METHODS

All methods can be found in the accompanying Transparent Methods supplemental file.

DATA AND SOFTWARE AVAILABILITY

The accession number of microarray data reported in this paper is GEO: GSE122374 and the accession number of RNA-seq data reported in this paper is GEO: GSE122346.

SUPPLEMENTAL INFORMATION

Supplemental Information can be found online at https://doi.org/10.1016/j.isci.2019.02.013.

ACKNOWLEDGMENTS

We thank Dr. Claudio J. Villanueva for the Prdm16 expression vector. This work was supported in part by AMED (Japan Agency for Medical Research and Development, Grant No. 16gm0510015h0004), and a Grant-in-Aid for Scientific Research on Innovative Areas from the Japanese Ministry of Education, Culture, Sports, Science, and Technology (MEXT, Grant No. 16H01413).

AUTHOR CONTRIBUTIONS

Y.L. performed most of the experiments. T.M. assisted with mouse experiments. K.Y. helped with analysis of ATF7-regulated immune genes. M.M. performed RNA-seq experiments. B.C. supplied monoclonal antibodies. S.I. conceived and supervised the whole study. S.I. and Y.L. wrote the manuscript.

DECLARATION OF INTERESTS

All authors declare no conflict of interest.

Received: November 30, 2018
Revised: January 24, 2019
Accepted: February 12, 2019
Published: March 29, 2019

REFERENCES

Bartelt, A., and Heeren, J. (2014). Adipose tissue browning and metabolic health. Nat. Rev. Endocrinol. *10*, 24–36.

Bordicchia, M., Liu, D., Amri, E.Z., Ailhaud, G., Dessi-Fulgheri, P., Zhang, C., Takahashi, N., Sarzani, R., and Collins, S. (2012). Cardiac natriuretic peptides act via p38 MAPK to induce the brown fat thermogenic program in mouse and human adipocytes. J. Clin. Invest. *122*, 1022–1036.

Brunmeir, R., Wu, J., Peng, X., Kim, S.Y., Julien, S.G., Zhang, Q., Xie, W., and Xu, F. (2016). Comparative transcriptomic and epigenomic analyses reveal new regulators of murine brown adipogenesis. PLoS Genet. *12*, e1006474.

Cao, W., Daniel, K.W., Robidoux, J., Puigserver, P., Medvedev, A.V., Bai, X., Floering, L.M., Spiegelman, B.M., and Collins, S. (2004). p38 mitogen-activated protein kinase is the central regulator of cyclic AMP-dependent transcription of the brown fat uncoupling protein 1 gene. Mol. Cell Biol. *24*, 3057–3067.

Cawthorn, W.P., Bree, A.J., Yao, Y., Du, B., Hemati, N., Martinez-Santibañez, G., and MacDougald, O.A. (2012). Wnt6, Wnt10a and Wnt10b inhibit adipogenesis and stimulate osteoblastogenesis through a β-catenin-dependent mechanism. Bone *50*, 477–489.

Charrière, G., Cousin, B., Arnaud, E., André, M., Bacou, F., Pénicaud, L., and Casteilla, L. (2003). Preadipocyte conversion to macrophage. Evidence of plasticity. J. Biol. Chem. *278*, 9850–9855.

Cousin, B., Munoz, O., Andre, M., Fontanilles, A.M., Dani, C., Cousin, J.L., Laharrague, P., Casteilla, L., and Penicaud, L. (1999). A role for preadipocytes as macrophage-like cells. FASEB J. *13*, 305–312.

Dempersmier, J., Sambeat, A., Gulyaeva, O., Paul, S.M., Hudak, C.S.S., Raposo, H.F., Kwan, H.-Y., Kang, C., Wong, R.H., and Sul, H.S. (2015). Cold-inducible Zfp516 activates UCP1 transcription to promote browning of white fat and development of brown fat. Mol. Cell *57*, 235–246.

Ferrari, A., Longo, R., Fiorino, E., Silva, R., Mitro, N., Cermenati, G., Gilardi, F., Desvergne, B., Andolfo, A., Magagnotti, C., et al. (2017). HDAC3 is a molecular brake of the metabolic switch supporting white adipose tissue browning. Nat. Commun. *8*, 93.

Gaire, M., Chatton, B., and Kedinger, C. (1990). Isolation and characterization of two novel, closely related ATF cDNA clones from HeLa cells. Nucleic Acids Res. *18*, 3467–3473.

Gupta, R.K., Arany, Z., Seale, P., Mepani, R.J., Ye, L., Conroe, H.M., Roby, Y.A., Kulaga, H., Reed, R.R., and Spiegelman, B.M. (2010). Transcriptional control of preadipocyte determination by Zfp423. Nature *464*, 619–623.

Gustafson, B., and Smith, U. (2006). Cytokines promote WNT signaling and inflammation and impair the normal differentiation and lipid accumulation in 3T3-L1 preadipocytes. J. Biol. Chem. *281*, 9507–9516.

Hai, T.W., Liu, F., Coukos, W.J., and Green, M.R. (1989). Transcription factor ATF cDNA clones: an extensive family of leucine zipper proteins able to selectively form DNA-binding heterodimers. Genes Dev. *3*, 2083–2090.

Harms, M., and Seale, P. (2013). Brown and beige fat: development, function and therapeutic potential. Nat. Med. *19*, 1252–1263.

Hogan, J.C., and Stephens, J.M. (2001). The identification and characterization of a STAT 1 binding site in the PPARgamma2 promoter. Biochem. Biophys. Res. Commun. *287*, 484–492.

Inagaki, T., Sakai, J., and Kajimura, S. (2016). Transcriptional and epigenetic control of brown and beige adipose cell fate and function. Nat. Rev. Mol. Cell Biol. *17*, 480–495.

Kajimura, S., and Saito, M. (2014). A new era in brown adipose tissue biology: molecular control of brown fat development and energy homeostasis. Annu. Rev. Physiol. *76*, 225–249.

Kajimura, S., Seale, P., Kubota, K., Lunsford, E., Frangioni, J.V., Gygi, S.P., and Spiegelman, B.M. (2009). Initiation of myoblast to brown fat switch by a PRDM16-C/EBP-β transcriptional complex. Nature *460*, 1154–1158.

Kissig, M., Ishibashi, J., Harms, M.J., Lim, H.W., Stine, R.R., Won, K.J., and Seale, P. (2017). PRDM16 represses the type I interferon response in adipocytes to promote mitochondrial and thermogenic programing. EMBO J. *36*, 1528–1542.

Kowenz-Leutz, E., and Leutz, A. (1999). A C/EBP β isoform recruits the SWI/SNF complex to activate myeloid genes. Mol. Cell *4*, 735–743.

Lai, B., Lee, J.E., Jang, Y., Wang, L., Peng, W., and Ge, K. (2017). MLL3/MLL4 are required for CBP/p300 binding on enhancers and super-enhancer formation in brown adipogenesis. Nucleic Acids Res. *45*, 6388–6403.

Lee, K., Um, S.H., Rhee, D.K., and Pyo, S. (2016). Interferon-alpha inhibits adipogenesis via regulation of JAK/STAT1 signaling. Biochim. Biophys. Acta *1860*, 2416–2427.

Lee, J.E., Park, Y.K., Park, S., Jang, Y., Waring, N., Dey, A., Ozato, K., Lai, B., Peng, W., and Ge, K. (2017). Brd4 binds to active enhancers to control

cell identity gene induction in adipogenesis and myogenesis. Nat. Commun. *8*, 2217.

Liu, Y., Maekawa, T., Yoshida, K., Furuse, T., Kaneda, H., Wakana, S., and Ishii, S. (2016). ATF7 ablation prevents diet-induced obesity and insulin resistance. Biochem. Biophys. Res. Commun. *478*, 696–702.

Maekawa, T., Jin, W., and Ishii, S. (2010a). The role of ATF-2 family transcription factors in adipocyte differentiation: antiobesity effects of p38 inhibitors. Mol. Cell. Biol. *30*, 613–625.

Maekawa, T., Sakura, H., Kanei-Ishii, C., Sudo, T., Yoshimura, T., Fujisawa, J., Yoshida, M., and Ishii, S. (1989). Leucine zipper structure of the protein CRE-BP1 binding to the cyclic AMP response element in brain. EMBO J. *8*, 2023–2028.

Maekawa, T., Kim, S., Nakai, D., Makino, C., Takagi, T., Ogura, H., Yamada, K., Chatton, B., and Ishii, S. (2010b). Social isolation stress induces ATF-7 phosphorylation and impairs silencing of the 5-HT 5B receptor gene. EMBO J. *29*, 196–208.

Maekawa, T., Liu, B., Nakai, D., Yoshida, K., Nakamura, K., Yasukawa, M., Koike, M., Takubo, K., Chatton, B., Ishikawa, F., et al. (2018). ATF7 mediates TNF-α-induced telomere shortening. Nucleic Acids Res. *46*, 4487–4504.

McLaughlin, T., Ackerman, S.E., Shen, L., and Engleman, E. (2017). Role of innate and adaptive immunity in obesity-associated metabolic disease. J. Clin.Invest *127*, 5–13.

Moisan, A., Lee, Y.K., Zhang, J.D., Hudak, C.S., Meyer, C.A., Prummer, M., Zoffmann, S., Truong, H.H., Ebeling, M., Kiialainen, A., et al. (2015). White-to-brown metabolic conversion of human adipocytes by JAK inhibition. Nat. Cell Biol. *17*, 57–67.

Nomura, N., Zu, Y.L., Maekawa, T., Tabata, S., Akiyama, T., and Ishii, S. (1993). Isolation and characterization of a novel member of the gene family encoding the cAMP response element-binding protein CRE-BP1. J. Biol. Chem. *268*, 4259–4266.

Ohno, H., Shinoda, K., Spiegelman, B.M., and Kajimura, S. (2012). PPARγ agonists induce a white-to-brown fat conversion through stabilization of PRDM16 protein. Cell Metab. *15*, 395–404.

Qatanani, M., Szwergold, N.R., Greaves, D.R., Ahima, R.S., and Lazar, M.A. (2009). Macrophage-derived human resistin exacerbates adipose tissue inflammation and insulin resistance in mice. J. Clin. Invest. *119*, 531–539.

Rajbhandari, P., Thomas, B.J., Feng, A.C., Hong, C., Wang, J., Vergnes, L., Sallam, T., Wang, B., Sandhu, J., Seldin, M.M., et al. (2018). IL-10 signaling remodels adipose chromatin architecture to limit thermogenesis and energy expenditure. Cell *172*, 218–233.e17.

Roh, H.C., Tsai, L.T.Y., Shao, M., Tenen, D., Shen, Y., Kumari, M., Lyubetskaya, A., Jacobs, C., Dawes, B., Gupta, R.K., et al. (2018). Warming induces significant reprogramming of beige, but not brown, adipocyte cellular identity. Cell Metab. *27*, 1121–1137.

Schoonjans, K., Staels, B., and Auwerx, J. (1996). The peroxisome proliferator activated receptors (PPARs) and their effects on lipid metabolism and adipocyte differentiation. Biochim. Biophys. Acta *1302*, 93–109.

Seale, P., Kajimura, S., Yang, W., Chin, S., Rohas, L.M., Uldry, M., Tavernier, G., Langin, D., and Spiegelman, B.M. (2007). Transcriptional control of brown fat determination by PRDM16. Cell Metab. *6*, 38–54.

Seong, K.H., Li, D., Shimizu, H., Nakamura, R., and Ishii, S. (2011). Inheritance of stress-induced, ATF-2-dependent epigenetic change. Cell *145*, 1049–1061.

Seong, K.H., Maekawa, T., and Ishii, S. (2012). Inheritance and memory of stress-induced epigenome change: roles played by the ATF-2 family of transcription factors. Genes Cells *17*, 249–263.

Shao, M., Ishibashi, J., Kusminski, C.M., Wang, Q.A., Hepler, C., Vishvanath, L., MacPherson, K.A., Spurgin, S.B., Sun, K., Holland, W.L., et al. (2016). Zfp423 maintains white adipocyte identity through suppression of the beige cell thermogenic gene program. Cell Metab. *23*, 1167–1184.

Sidossis, L., and Kajimura, S. (2015). Brown and beige fat in humans: thermogenic adipocytes that control energy and glucose homeostasis. J. Clin. Invest. *125*, 478–486.

Sun, W., Dong, H., Becker, A.S., Dapito, D.H., Modica, S., Grandl, G., Opitz, L., Efthymiou, V., Straub, L.G., Sarker, G., et al. (2018). Cold-induced epigenetic programming of the sperm enhances brown adipose tissue activity in the offspring. Nat. Med. *24*, 1372–1383.

Villanueva, C.J., Vergnes, L., Wang, J., Drew, B.G., Hong, C., Tu, Y., Hu, Y., Peng, X., Xu, F., Saez, E., et al. (2013). Adipose subtype-selective recruitment of TLE3 or Prdm16 by PPARγ specifies lipid storage versus thermogenic gene programs. Cell Metab. *17*, 423–435.

Villanueva, C.J., Waki, H., Godio, C., Nielsen, R., Chou, W.L., Vargas, L., Wroblewski, K., Schmedt, C., Chao, L.C., Boyadjian, R., et al. (2011). TLE3 is a dual-function transcriptional coregulator of adipogenesis. Cell Metab. *13*, 413–427.

Wang, L., Xu, S., Lee, J.E., Baldridge, A., Grullon, S., Peng, W., and Ge, K. (2013). Histone H3K9 methyltransferase G9a represses PPARγ expression and adipogenesis. EMBO J. *32*, 45–59.

Yao, L., Cui, X., Chen, Q., Yang, X., Fang, F., Zhang, J., Liu, G., Jin, W., and Chang, Y. (2017). Cold-inducible SIRT6 regulates thermogenesis of brown and beige fat. Cell Rep. *20*, 641–654.

Yoshida, K., Maekawa, T., Zhu, Y., Renard-Guillet, C., Chatton, B., Inoue, K., Uchiyama, T., Ishibashi, K., Yamada, T., Ohno, N., et al. (2015). The transcription factor ATF7 mediates lipopolysaccharide-induced epigenetic changes in macrophages involved in innate immunological memory. Nat. Immunol. *16*, 1034–1043.

Zhao, M., and Chen, X.L. (2015). Effect of lipopolysaccharides on adipogenic potential and premature senescence of adipocyte progenitors. Am. J. Physiol. Endocrinol. Metab. *309*, E334–E344.

ISCI, Volume *13*

Supplemental Information

The Transcription Factor ATF7 Controls Adipocyte Differentiation and Thermogenic Gene Programming

Yang Liu, Toshio Maekawa, Keisuke Yoshida, Masafumi Muratani, Bruno Chatton, and Shunsuke Ishii

Supplementary Figures

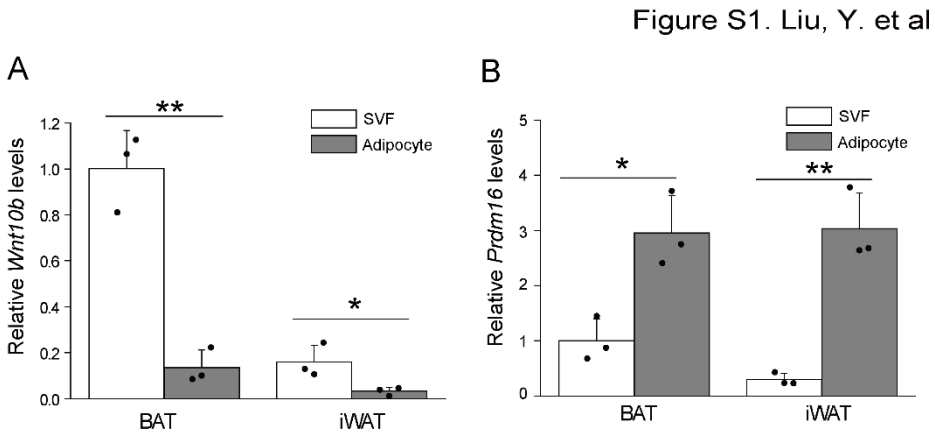

Figure S1. *Wnt10b* and *Prdm16* gene expression in mature adipocytes and stromal vascular cells, Related to Figure 1.

(A, B) Relative mRNA levels of *Wnt10b* (**A**) and *Prdm16* (**B**) in mature adipocytes and stromal vascular cells isolated from BAT and iWAT (n = 3, three biological replicates). Data are presented as means ± SD. Statistical analysis was performed using two-tailed unpaired Student's t-tests. *$p < 0.05$; **$p < 0.01$.

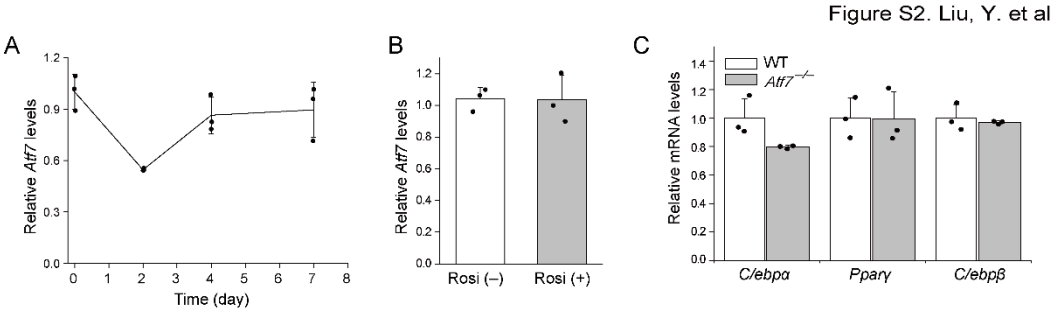

Figure S2. Rosiglitazone rescues the defective adipogenic potential of *Atf7*$^{-/-}$ preadipocytes, Related to Figure 1.

(A) *Atf7* gene expression during the differentiation time course of primary iWAT preadipocytes in the presence of rosiglitazone (Rosi; n = 3, three biological replicates). **(B)** *Atf7* gene expression levels in differentiated preadipocytes treated with or without Rosi (n = 3, three biological replicates). **(C)** Expression levels of adipogenic genes *C/ebpβ*, *Pparγ*, and *C/ebpα* in differentiated WT and *Atf7*$^{-/-}$ preadipocytes treated with Rosi (n = 3, three biological replicates). Data are presented as means ± SD. Statistical analysis was performed using two-tailed unpaired Student's t-tests.

Figure S3. Liu, Y. et al

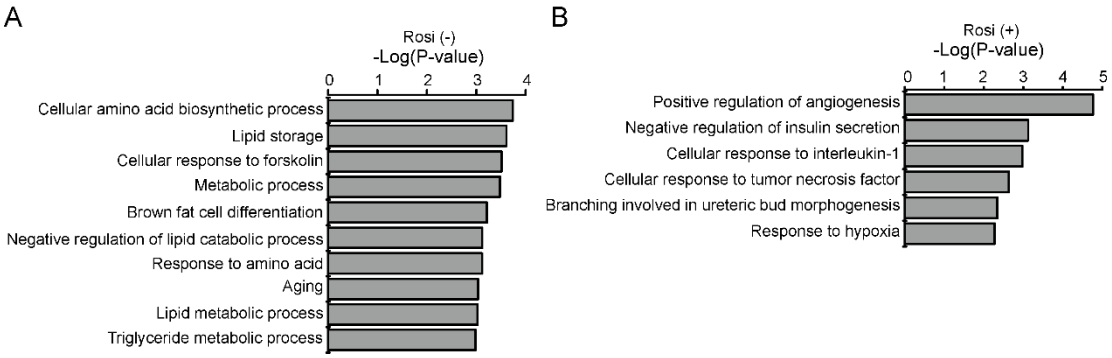

Figure S3. GO analysis for down-regulated genes in the *Atf7*$^{-/-}$ adipocytes, Related to Figure 2.

(A, B) Gene Ontology (GO) pathways (Biological Process category) enriched in down-regulated genes in differentiated *Atf7*$^{-/-}$ primary iWAT preadipocytes compared with WT controls in the absence (**A**) or presence (**B**) of rosiglitazone (Rosi).

Figure S4. Liu, Y. et al

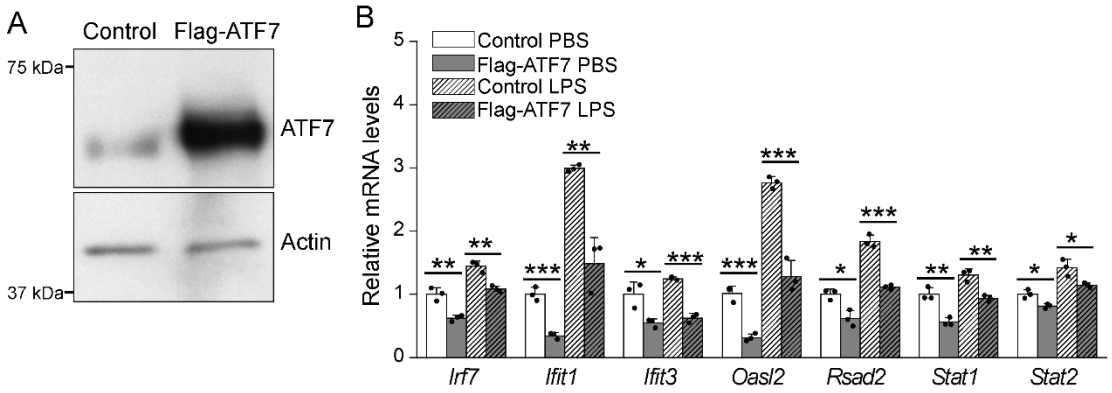

Figure S4. Overexpression of ATF7 suppresses the induction of ISGs in C3H10T1/2 cells, Related to Figure 2.

(A) Overexpression of ATF7 in C3H10T1/2 confirmed by immunoblotting using an antibody against ATF7. **(B)**Relative mRNA levels of ISGs in control and ATF7-overexpressing C3H10T1/2 cells before and after LPS treatment (n = 3, three biological replicates). Data are presented as means ± SD. Statistical analysis was performed using two-tailed unpaired Student's t-tests. *$p < 0.05$; **$p < 0.01$; ***$p < 0.001$.

Figure S5. Liu, Y. et al

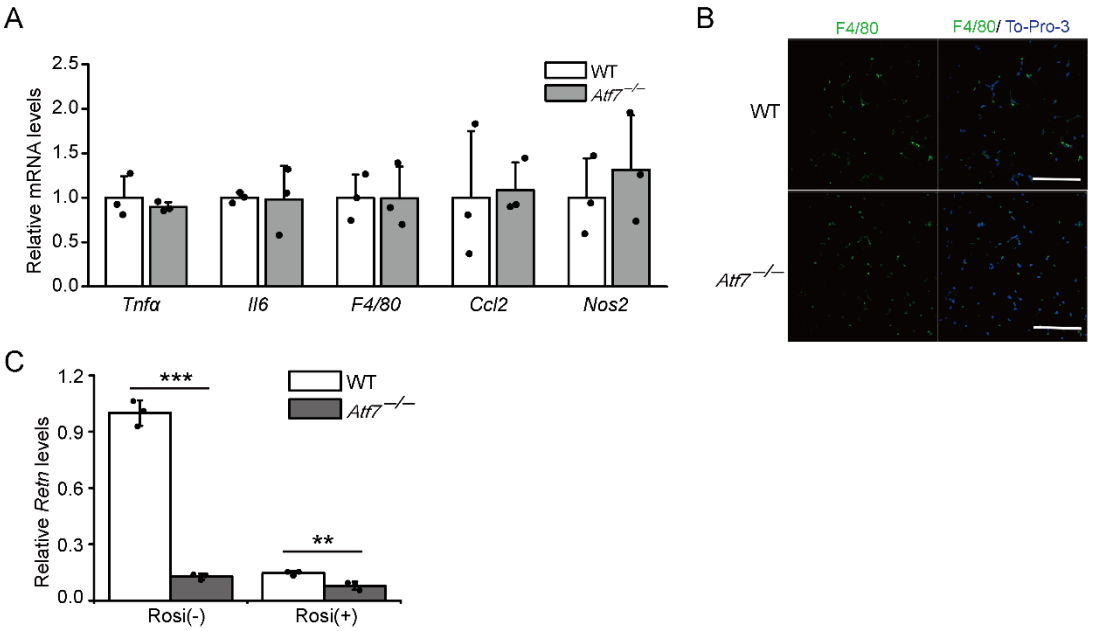

Figure S5. Loss of ATF7 does not affect the inflammation of inguinal white adipose tissue, Related to Figure 2.

(A) Relative mRNA levels of pro-inflammatory genes in iWAT from WT and *Atf7*$^{-/-}$ littermates (n = 3, three biological replicates). **(B)** Representative images of macrophages as assessed by F4/80 Immunofluorescence in iWAT from WT and *Atf7*$^{-/-}$ littermates. The sections were stained with anti-F4/80 antibodies (green) and cell nuclei were stained by using To-Pro-3 (blue). Confocal images were taken at ×40 magnification. Scale bar = 100μm. **(C)** mRNA expression of *Retn* in differentiated (D7) WT and *Atf7*$^{-/-}$ primary iWAT preadipocytes in the presence or absence of Rosi. (n = 3, three biological replicates). Data are presented as means ± SD. Statistical analysis was performed using two-tailed unpaired Student's t-tests. $^{**}p < 0.01$; $^{***}p < 0.001$.

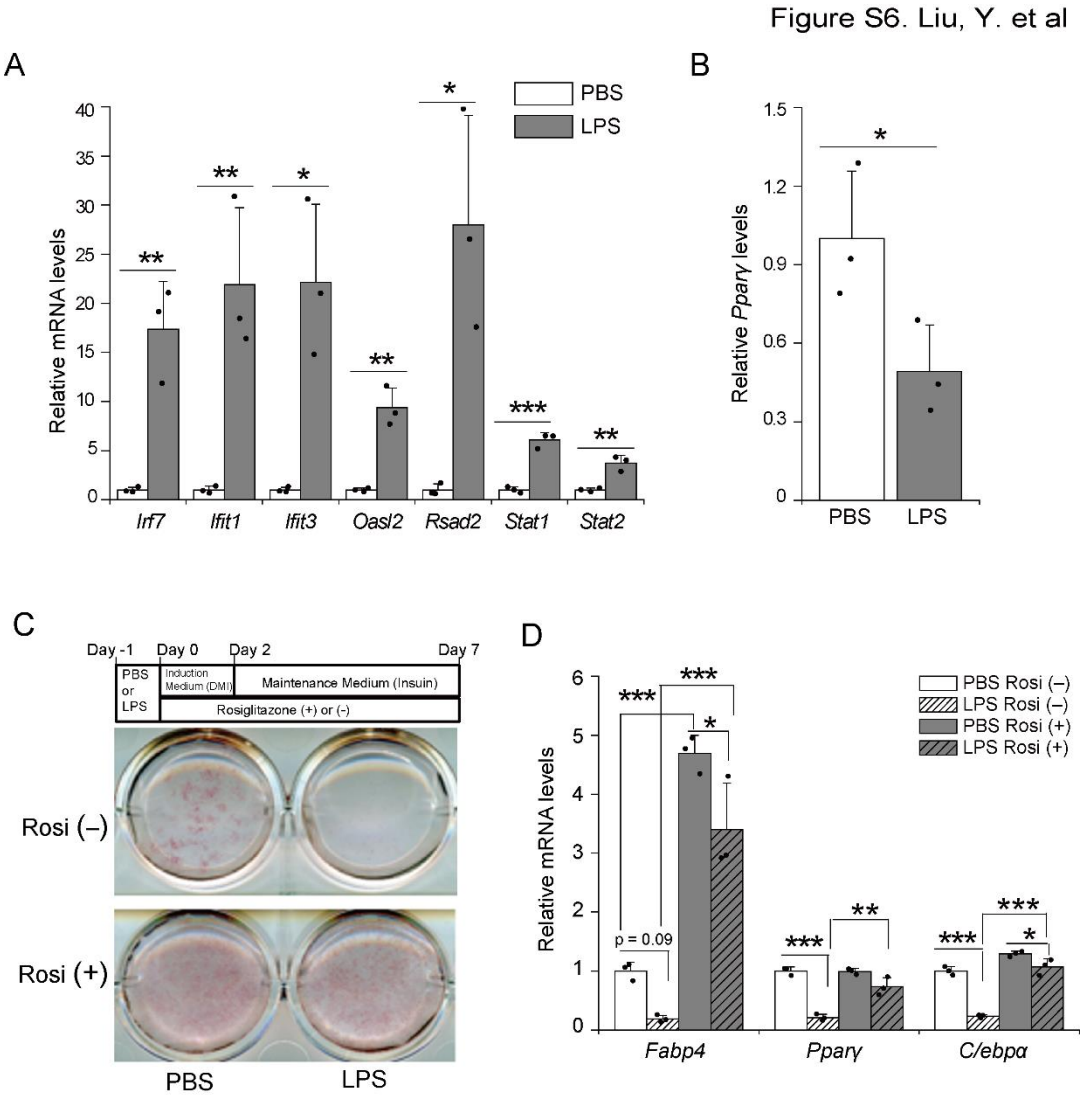

Figure S6. Induction of ISGs expression in preadipocytes by LPS treatment impairs adipogenesis, Related to Figure 3.

(A, B) Relative mRNA levels of ISGs (**A**) and *Pparγ* (**B**) measured in preadipocytes after LPS or PBS treatment for 24 hr (n = 3, three biological replicates). Data are presented as means ± SD. Statistical analysis was performed using two-tailed unpaired Student's t-tests. **p* < 0.05; ***p* < 0.01; ****p* < 0.001. **(C, D)** Oil Red O staining (**C**) and adipogenic gene expression levels **(D)** in differentiated primary iWAT preadipocytes (D7, n = 3, three biological replicates) treated with LPS or PBS prior to the induction of differentiation. Data are presented as means ± SD. Statistical analysis was performed using two-way ANOVA followed by Holm-Sidak multiple comparison tests. **p* < 0.05; ***p* < 0.01; ****p* < 0.001.

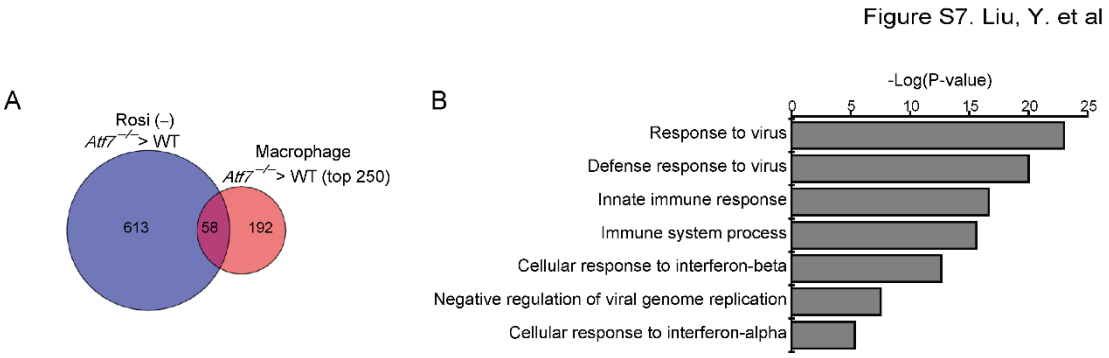

Figure S7. ATF7 represses expression of ISGs in both macrophages and preadipocytes, Related to Figure 4.

(A) Venn diagram showing the number of overlapping up-regulated genes induced by loss of ATF7 in macrophages and adipocytes. **(B)** Pathway analysis of overlapping up-regulated genes in *Atf7*$^{-/-}$ macrophages and adipocytes.

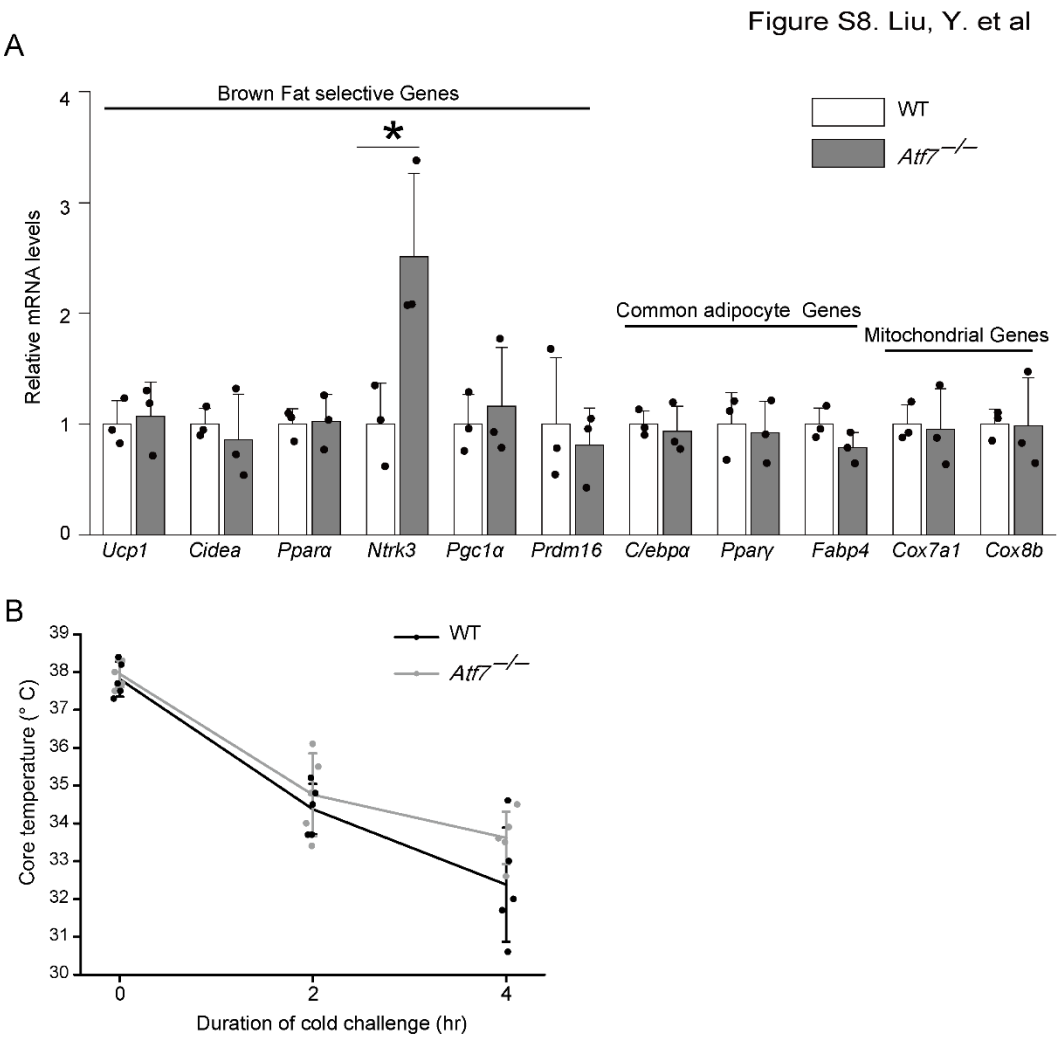

Figure S8. Loss of ATF7 does not promote thermogenic gene programming in BAT and acute cold tolerance, Related to Figure 6.

(A) Expression of brown fat-selective genes, common adipocyte genes, and mitochondrial genes in BAT from WT and *Atf7*$^{-/-}$ littermates (n = 3, three biological replicates). **(B)** Core body temperature of WT and *Atf7*$^{-/-}$ littermates during acute cold exposure from standard housing at 23°C to 4 °C (n = 5, five biological replicates). Data are presented as means ± SD. Statistical analysis was performed using two-tailed unpaired Student's t-tests. *$p < 0.05$.

Table S1. Sequences of primers used for RT-PCR, Related to Figures 1, 2, 3, 4, 5, 6, and 7.

Gene	**Forward primer (5'–3')**	**Reverse primer (5'–3')**
Atf7	GGGTGTCCTCCCTGGAAAAG	TCAGCTGAGCCACCTCATTG
Fabp4	AAGGTGAAGAGCATCATAACCCT	TCACGCCTTTCATAACACATTCC
Pparg	GCATGGTGCCTTCGCTGA	TGGCATCTCTGTGTCAACCATG
Cebpa	CAAGAACAGCAACGAGTACCG	GTCACTGGTCAACTCCAGCAC
Cebpb	AAGCTGAGCGACGAGTACAAGA	GTCAGCTCCAGCACCTTGTG
Stat2	TCCTGCCAATGGACGTTCG	GTCCCACTGGTTCAGTTGGT
Oasl2	TCTGGAGCTGCTGACCATCTACG	CATCACGGCTACGAACCCTTCATC
Ifit3	GCTCAGCCCACACCCAGCTTT	AGATTCCCGGTTGACCTCACTCAT
Ifit1	AGAACAGCTACCACCTTTAC	TTCTTGATGTCAAGGAACTG
Rsad2	CTGTGCGCTGGAAGGTTT	ATTCAGGCACCAAACAGGAC
Stat1	GGCGTCTATCCTGTGGTACAACA	GTGACTGATGAAAACTGCCAACTC
Irf7	GCCTTGGGTTCCTGGATGTGA	TGGGGCCATGGGGCTGTA
36b4	GCTCCAAGCAGATGCAGCA	CCGGATGTGAGGCAGCAG
Wnt10b	GCTGACTGACTCGCCCACCG	AAGCACACGGTGTTGGCCGT
Ucp1	ACTGCCACACCTCCAGTCATT	CTTTGCCTCACTCAGGATTGG
Cidea	TGCTCTTCTGTATCGCCCAGT	GCCGTGTTAAGGAATCTGCTG
Pgc1a	CCCTGCCATTGTTAAGACC	TGCTGCTGTTCCTGTTTTC
Prdm16	CAGCACGGTGAAGCCATT C	GCGTGCATCCGCTTGTG
Cox8b	GAACCATGAAGCCAACGACT	GCGAAGTTCACAGTGGTTCC

Cox7a1	CAGCGTCATGGTCAGTCTGT	AGAAAACCGTGTGGCAGAGA
Ntrk3	TGGCTCACACTGATCTCTGG	GCCAGAGCCTTTACTGCATC
Elovl3	TTCTCACGCGGGTTAAAAATGG	TCTCGAAGTCATAGGGTTGCAT
Ppara	ACTACGGAGTTCACGCATGTG	TTGTCGTACACCAGCTTCAGC
Nos2	GGCTGTCACGGAGATCAATG	TCTGAGGCTGTGTGGTGGTC
Retn	CTGTCCAGTCTATCCTTGCACAC	CAGAAGGCACAGCAGTCTTGA
Il6	TGAGAAAAGAGTTGTGCAATGG	GGTACTCCAGAAGACCAGAGG
Tnfa	GACCCTCACACTCAGATCATCTTCT	CCTCCACTTGGTGGTTTGCT
F4/80	CTTTGGCTATGGGCTTCCAGTC	GCAAGGAGGACAGAGTTTATCGTG
Ccl2	AAGGAATGGGTCCAGACATAC	CTGAAGACCTTAGGGCAGAT

Table S2. Sequences of primers used for ChIP-qPCR, Related to Figures 4 and 8.

Primer	**Forward primer (5'–3')**	**Reverse primer (5'–3')**
*Stat1*_Promoter	GGAACAGCCGGCCAATC	AAAGTACCGGGCAGGAAAAAAG
*Ucp1*_enhancer-12kb	GCAACCCTCTCCCATCAGTG	GCCTAACACCGTGCTTCTCA
*Ucp1*_enhancer-5kb	TGCAACCCCTCACCTTTTAC	CTCCTTCCATCATCCCTTCA
*Ucp1*_enhancer-2.5kb	AAGAACACGGACACTAGG	GAAAGGTGACGACTAGTTC

Transparent Methods

Animals

ATF7-deficient (*Atf7*$^{-/-}$) mice were generated as described previously (Maekawa et al., 2010). *Atf7*$^{-/-}$ and wild-type (WT) littermates derived from Atf7 heterozygotes in a C57BL/6 background were used in this study. Experiments were conducted in accordance with the Guidelines of the Animal Care and Use Committee of the RIKEN Institute. No randomization of animals was used. The investigators were not blinded to group allocation of mice during the experiments.

Antibodies

Mouse monoclonal antibodies (1A7 and 2F10) against ATF7 were supplied by Dr. Bruno Chatton. Antibodies recognizing Flag-tag (F3165) and HA-tag (ab9110) were purchased from Sigma and Abcam, respectively. A rabbit polyclonal phosphor-specific antibody against ATF2-Thr71/ATF7-Thr53 (#9221) was purchased from Cell Signaling. A mouse monoclonal antibody recognizing H3K9me2 (MABI0307) was purchased from MBL. Antibodies against actin (I-19, sc-1616), glyceraldehyde-3-phosphate dehydrogenase (GAPDH; FL-335, sc-25778), tubulin (B-7, sc-5286), F4/80 (3H2113, sc-71088), and C/EBPβ (C-19, sc-150) were purchased from Santa Cruz Biotechnology. A rabbit polyclonal antibody recognizing UCP1 (Ab10983) was purchased from Abcam. Antibodies against Prdm16 (AF6295) and G9a (A8620A) were purchased from R&D Systems and Perseus Proteomics, respectively.

Isolation of mature adipocyte and stromal vascular cells

Fat tissues were dissected from 6–8-week-old male mice and digested in digestion buffer containing

10 mM $CaCl_2$, 2% bovine serum albumin (BSA), and 1 mg/ml collagenase (SIGMA, C0130) in phosphate-buffered saline (PBS) for 60 min at 37°C, followed by washing with DMEM/F12 medium (Life Technologies/Gibco, #10565018) containing 10% fetal bovine serum (FBS). Digested tissues were filtered with 70 μM cell strainers, and the flow-through was centrifuged at 450 × g for 5 min. Stromal vascular cells were pelleted, and mature adipocytes were separated as the floating layer.

Primary cell culture and differentiation

To isolate primary iWAT preadipocytes, inguinal iWATs were isolated from 4–6-week-old male mice, and stromal vascular cells were isolated as described above. Cells were washed with PBS twice for 2 h each time after seeding on plates, then cultured in DMEM/F12 medium with 10% FBS until confluence. To induce cell differentiation, confluent cells were challenged for 2 days in induction medium (DMEM/F12 with 10% FBS, 5 μg/ml insulin, 1 μM dexamethasone, 0.5 mM isobutylmethylxanthine). Subsequently, cells were cultured in maintenance medium (DMEM/F12 with 10% FBS, 5 μg/ml insulin) for 5 more days, and medium was replaced every other day. Cells were incubated in the presence or absence of 1 μM rosiglitazone (Rosi) for the entire differentiation time course. To activate β-adrenergic receptor signaling, cells were treated with 2 μM isoproterenol for 4 hr. To examine the effects of innate immune responses on adipocyte differentiation, cells were incubated with 0.5 μg/ml LPS (L4391, Sigma) for 24 hr prior to differentiation, or IFN-α (500 U/ml, #130093; Miltenyi Biotec) during the entire time course of differentiation.

C3H10T1/2 cell differentiation

The C3H10T1/2 cell line (clone 8) was purchased from the RIKEN Bio-Resource Center (Saitama, Japan) and cultured in DMEM medium containing 10% FBS. To induce brown/beige cell differentiation, cells were incubated for 2 days in DMEM medium supplemented with 10% FBS, 5 μg/ml insulin, 1 μM dexamethasone, 0.5 mM isobutylmethylxanthine, and 1 μM Rosi, and maintained for 5 days in DMEM medium containing 10% FBS, 5 μg/ml insulin, and 1 μM Rosi. To generate ATF7-overexpressing cells, C3H10T1/2 cells were infected with pLenti6.3-CMV_Flag_ATF7 or pLenti6.3-CMV_dsRed virus, generated using the vector plenti6.3/TO/V5-GW/lacZ (Life Technologies), and subsequently selected in medium containing 10 μg/ml blasticidin (#15205; Sigma).

Co-immunoprecipitation

293T cells were transfected with HA-Prdm16, Flag-ATF7, and C/EBPβ-HIS expression plasmids using X-tremeGENE HP DNA Transfection Reagent (Sigma). Cells were lysed with NETN buffer (20 mM TRIS pH 8.0, 150 mM sodium chloride, 0.5% NP-40, 1 mM EDTA, protease inhibitors). Lysates were incubated with antibody recognizing the HA-tag overnight at 37°C, then incubated with Protein A Dynabeads (Invitrogen) for 4 hr. Beads were washed four times with NETN buffer, and bound protein was eluted with 2× sodium dodecyl sulfate (SDS) sample buffer.

To confirm the interaction between endogenous G9a and ATF7 in primary iWAT preadipocytes, the experiment was performed as described previously with minor modifications (Yoshida et al., 2015). Briefly, nuclei were extracted with hypotonic buffer A (10 mM HEPES pH 7.9, 10 mM KCl, 0.1 mM EDTA, 0.1 mM EGTA, 1 mM DTT, 0.6% NP-40, 0.1 μM okadaic acid, protease inhibitors) and incubated for 15 min in HS IP buffer (50 mM TRIS-HCl pH 7.5, 450 mM NaCl, 1 mM EDTA,

0.5% NP-40, 0.1 μM okadaic acid, protease inhibitors). After the salt concentration was adjusted to 150 mM, the solution was incubated with Protein G Dynabeads (Invitrogen) and anti-ATF7 (2F10) or control IgG overnight. Beads were washed with IP buffer (50 mM TRIS-HCl pH 7.5, 150 mM NaCl, 1 mM EDTA, 0.5% NP-40, 0.1 μM okadaic acid, protease inhibitors), and protein was eluted with 2× SDS sample buffer. Analysis of the interaction between C/EBPβ and ATF7 in beige adipocytes (C3H10T1/2, D4) was performed using the same method.

Western blotting

Protein extracts were prepared by homogenization in radioimmunoprecipitation (RIPA) buffer (50 mM TRIS-HCl pH 8.0, 150 mM sodium chloride, 0.1% SDS, 0.5% sodium deoxycholate, 1% NP-40, 0.1 μM okadaic acid, and protease inhibitors). Proteins were separated by SDS-polyacrylamide gel electrophoresis (PAGE) and transferred to a polyvinylidene fluoride (PVDF) membrane. After treatment with primary antibody at 4°C overnight, blots were incubated with a peroxidase-conjugated secondary antibody (Santa Cruz Biotechnology) followed by ECL detection (GE Healthcare) according to the manufacturer's instructions.

Quantitative RT-PCR analysis

Total RNA was extracted using TRIzol (Invitrogen), and RT-PCR was performed on a 7500 Fast Real-time PCR System using OneStep SYBR Green PCR mix (TaKaRa) following the manufacturer's instructions. The reference gene *36B4* was used as an internal control for normalization, and data were analyzed using the 2–ΔΔCt method. Primer sequences are listed in Table S1.

Chromatin immunoprecipitation

Primary iWAT preadipocytes and adipocytes were fixed with 1% formaldehyde in medium for 10 min, and crosslinking was quenched by addition of glycine at a final concentration of 125 mM. Lysed cells were sonicated in SDS lysis buffer (50 mM TRIS-HCl pH 8.0, 10 mM EDTA, 1% SDS, and protease inhibitors). For immunoprecipitation, equal aliquots of cell lysates were incubated with the indicated antibodies overnight at 4°C, followed by incubation with Protein A Dynabeads for 4 hr, then washed four times with wash buffer (50 mM HEPES pH 7.0, 0.5 M LiCl, 1 mM EDTA, 0.7% sodium deoxycholate, 1% NP-40) and twice with TE buffer (10 mM TRIS-HCl pH 8.0, 1 mM EDTA). Immunocomplexes were eluted in elution buffer, and crosslinking was performed by overnight incubation at 65°C. Precipitated DNA was analyzed by real-time PCR with primers listed in Table S2.

Microarray analysis

Inguinal WAT samples were isolated from 5-week-old male mice, and total RNA was extracted using TRIzol (Invitrogen). Single-strand cDNA was prepared and labeled using a WT Expression Kit (Ambion, Invitrogen Life Technologies, Carlsbad, CA, USA) and a WT terminal labeling kit (Ambion) according to the manufacturer's instructions. Samples were analyzed by microarray using the mouse Gene 1.0 ST Array (Affymetrix). Data were analyzed using the Linear Models for Microarray Data (Limma) package (Smyth, 2005). Differentially expressed genes (DEGs) were defined with a *p*-value of ≤ 0.05 and an absolute Log2 fold-change of ≥ 0.6. Gene Ontology (GO) analysis was performed on up-regulated genes using DAVID (Huang et al., 2009), and the top

significantly over-represented terms from GOTERM_BP_ DIRECT were identified. The accession number of microarray data reported in this paper is GEO: GSE122374.

RNA-seq

RNA was isolated from differentiated adipocytes (n = 2, two biological replicates) using TRIzol reagent. RNAseq libraries were prepared with a NEBNext rRNA Depletion Kit and a NEBNext Ultra Directional RNA Library Preparation Kit (New England Biolabs, Ipswich, MA), and then 2 × 36 base pair-end sequencing was performed using NextSeq500 (Illumina, San Diego, CA) by Tsukuba i-Laboratory LLP (Tsukuba, Ibaraki, Japan). RNA-seq reads were aligned against the UCSC mm10 database using HISAT (Kim et al., 2015), and Transcript assembly was performed with Cufflinks (Trapnell et al., 2012). Differential expression analysis was performed using Cuffdiff (Trapnell et al., 2012), and GO analysis was carried out as described above. The accession number of RNA-seq data reported in this paper is GEO: GSE122346.

Histology

Adipose tissues were isolated from mice and fixed in 4% paraformaldehyde overnight at 4°C. Paraffin sections (5 μm thick) were sliced, deparaffinized, rehydrated, and stained with hematoxylin and eosin. Immunohistochemical analysis was performed according to the ABC method using PK-6101 (Vector Laboratories) following the manufacturer's instructions. Briefly, sections were treated with rabbit polyclonal anti-UCP1 primary antibody (1:200 dilution) after antigen retrieval and blocked with blocking buffer (PBS containing 2% bovine serum albumin and 10% normal serum). Sections were then incubated with biotinylated anti-rabbit antibody, followed by incubation with

avidin-biotin-horseradish peroxidase complex. Labeling was detected with 2,3'-diaminobenzidine tetrahydrochloride (DAB) and examined using a light microscope.

The inflammation of adipose tissues were examined by staining the sections with the macrophage specific anti-F4/80 and Alexa Fluor 488-conjugated monkey anti-rat IgG (H+L). Cell nuclei were staining with To-Pro-3. Fluorescent images were taken on a Zeiss LSM laser scanning microscope.

Oil Red O staining

Differentiated cells were washed with PBS twice and fixed with 10% formalin for 1 hr. Cells were then washed with 60% isopropanol followed by staining with Oil Red O working solution for 30 min. Cells were finally washed with water four times, and images were scanned.

Statistical analysis

All statistical analyses were performed using Prism 8 (GraphPad Software, Inc). Data are presented as the mean ± standard deviation (SD). Two-tailed unpaired Student's t-tests were performed for comparison of two groups, and multiple comparisons were carried out by two-way analysis of variance (ANOVA) with Holm-Sidak post-hoc tests. A p-value <0.05 was considered statistically significant. The sample size was not determined by statistical methods, and no samples or animals were excluded from the analysis.

Supplemental References

Huang D.W., Sherman B.T. and Lempicki R.A., Systematic and integrative analysis of large gene

lists using DAVID bioinformatics resources, *Nat. Protoc*. **4**, 2009, 44–57.

Kim D., Langmead B. and Salzberg S.L., HISAT: a fast spliced aligner with low memory requirements, *Nat. Methods* **12**, 2015, 357–360.

Smyth G.K., Limma: linear models for microarray data, In: Gentleman R., Carey V., Dudoit S., Irizarry R. and Huber W., (Eds.), *Bioinformatics and Computational Biology Solutions Using R and Bioconductor*, 2005, Springer, 397–420.

Trapnell C., Roberts A., Goff L., Pertea G., Kim D., Kelley D.R., Pimentel H., Salzberg S.L., Rinn J.L. and Pachter L., Differential gene and transcript expression analysis of RNA-seq experiments with TopHat and Cufflinks, *Nat. Protoc*. **7**, 2012, 562–578.